

Reprinted from

theoretical and applied fracture mechanics

Theoretical and Applied Fracture Mechanics 22 (1995) 97-114

Characterization of strain-induced damage in composites based on the dissipated energy density Part II. Composite specimens and naval structures

P.W. Mast, G.E. Nash ¹, J.G. Michopoulos ^{*}, R. Thomas ², R. Badaliane, I. Wolock [†]

*Mechanics of Materials Branch, Materials Science and Technology Division, U.S. Naval Research Laboratory,
Washington, DC 20375, USA*





Characterization of strain-induced damage in composites based on the dissipated energy density

Part II. Composite specimens and naval structures

P.W. Mast, G.E. Nash ¹, J.G. Michopoulos ^{*}, R. Thomas ², R. Badaliane, I. Wolock [†]

*Mechanics of Materials Branch, Materials Science and Technology Division, U.S. Naval Research Laboratory,
Washington, DC 20375, USA*

Abstract

Completed in Part I of this work are the description of the basic scheme and formulation by characterizing the damage behavior of composites by application of the dissipated energy density. Part II presents the development of a structural response simulator tool for composite structures subjected to different combinations of boundary displacements and loads. A presentation of distributions of dissipated energy density for the different load combinations on the specimens used in the In-Plane Loader (IPL) procedure described in Part I follows. Simulated response for several structures of interest to the Navy is also presented. They include a ship's mast and a cylindrical shell representing an idealized section of a submarine hull. Displayed are spatial maps of the dissipated energy density (softening maps) for various loading amplitudes. These softening maps reflect how energy is consumed by the different failure events within the structure.

1. Introduction

The use of composite materials in structural components has increased dramatically in recent years as their cost of production continues to decline and advances in composite design methodology become increasingly wide spread. As applications become more demanding, the need for reliable prediction of their mechanical

properties and behavior is becoming ever more important.

Extensive efforts have been made [1-5] in recent years to identify the various modes of damage in composite materials. Also refer to the references in Part I [6]. The primary finding of most of these investigations was that macroscopic fracture was usually preceded by an accumulation of the different types of microscopic damage and occurred by the coalescence of this small-scale damage into macroscopic cracks. Additionally, it was generally found that analyses based on classical fracture mechanics did not adequately model the damage effects and did not provide a satisfactory degree of predictive capability.

A more practical approach to modeling failure

^{*} Corresponding author. E-mail yiannis@prologos.nrl.navy.mil.

¹ Retired.

² Presently with FMT.

[†] Deceased

behavior in composites is to quantify the damage development on a continuum basis and relate it to the material constitutive behavior. The goal of such an approach is to permit accurate modeling of the progressive loss of stiffness and concomitant inelastic behavior caused by the underlying micromechanisms of damage [7–10]. Such a model for composite failure behavior requires a large parameter space for its description if it is to represent physical fact in a high-fidelity, objective manner. The model must be generic and phenomenological in nature and must rely on extensive sets of experimental data to identify the model parameters. Only after these parameters are determined can the model be related to particular failure mechanisms.

Following the basic scheme and formulation developed Part I [6] for relating the dissipated energy density as a function of strain in terms of a set of known basis functions and a set of undetermined coefficients. The task is then to estimate these coefficients. To accomplish this, a number of test specimens are first subjected to a range of prescribed combinations of in-plane loads using the In-Plane Loader [6]. These loads induce a wide range of internal strain states in the specimens. These states approximately encompass those expected in typical structural components under service loading conditions. The boundary displacements and boundary loads are measured for each load combination, and are used to compute the energy dissipated internally in the specimens caused by strain-induced damage for each test. The strain fields associated with each of the load combinations are also determined by means of a linear finite element analysis using the constitutive properties of the undamaged (virgin) material. The computation, therefore, neglects the effects of stiffness changes induced by the internal damage, but should be sufficiently accurate provided that no large-scale stress redistribution occurs during the tests. Analytic estimates of the dissipated energy are then computed in terms of the unknown coefficients for each test using the representation of the dissipation function, the computed strain fields, and the fact that the volume integral of the dissipation function equals the dissipated energy.

Finally, the undetermined coefficients in the dissipation function representation are determined by minimizing the difference between the experimentally measured and the analytic estimates of the dissipated energy for all the tests.

The aforementioned procedure is a deconvolution procedure in the sense that the goal is to extract a material property (the dissipated energy density function) from information obtained from the material in a particular physical configuration, namely the specimen, and, thus, it is necessary to factor out specimen geometry effects. By taking this approach, the resulting dissipated energy density function can be applied to any structural configuration, and used to develop material softening (stiffness reduction) maps for any structure (again, assuming a negligible amount of stress redistribution caused by internal damage).

Applicability of the model is demonstrated by describing a computational approach packaged as a material response simulator and its use in simulating the structural response of several structures of interest. These are the test specimen itself, a ship's mast, and a cylindrical shell representing an idealized section of a submarine hull. A number of different composite material systems are considered and spatial maps of the dissipation function (softening maps) are produced for various loading magnitudes. These softening maps illustrate how the energy consumed by the various internal failure events is dissipated within the structure.

2. Structural response simulator

The idea of a structural response simulator will be developed and it will be shown how the computed energy dissipation functions can be used within the simulator to design structural components and predict various aspects of their mechanical behavior. Because dissipated energy is taken as a measure of internal structural damage, one use of a simulator would be for structural designers to examine simulated spatial dissipated energy distributions to form selection criteria for evaluating the structural response of structures at a particular state of the design process.

Material system designers could also use a simulator to generate spatial dissipated energy maps from which they could determine the material response of a composite material system, and then select sets of manufacturing parameters to optimize the damage tolerance of new systems. Using the simulator to analyze material softening distribution patterns could also assist in selecting a material system for a particular structural design. Finally, a structural response simulator could even be used to qualify material systems by using far more realistic qualification criteria than are currently employed, e.g., strength or fracture toughness, which only indirectly and partially assess some qualitative aspects of the materials. Indeed, it is shown in this section that higher strength does not necessarily imply better damage tolerance.

In order to develop a tool for addressing the types of problems discussed above, a structural response simulator was created that takes user-specified geometries, materials, and loading conditions as inputs and creates spatial material distributions of local stiffness loss using the experimentally obtained dissipated energy functions. Fig. 1 shows the architecture of the structural response simulator in the configuration used to generate the results presented in this section. It has since evolved into a much more sophisticated

form and its design now includes such advanced functionality as user-simulator interaction modelling via artificial neural nets and other techniques.

The Fig. 1 block diagram shows the structure of the simulator in terms of component subsystems. The user interface was created by writing a library of function calls using the "PATRAN Command Language" (PCL) that allows the user to specify the geometry, the material, and the loading for the structure of interest. Visualization capabilities are provided through PDA's "PATRAN" 2.4 solid modeling package. A finite element idealization of the structure is achieved through appropriate use of PCL and all relevant model information is stored in "PATRAN" neutral files on the mass storage memory resources of the computer system hosting the simulator, which is currently a "Silicon Graphics Indigo" with 32 Mb of RAM and 2.5 GB of mass storage memory. The actual finite element analysis is performed by using the "ABAQUS" finite element code on a CRAY YMP/EL mini supercomputer, and assuming linear elastic behavior. The objective of the finite element analysis is to generate the strain field in the structure for the initial elastic state. The data required by "ABAQUS" are provided by the "PATABA" process that translates the "PATRAN" neutral

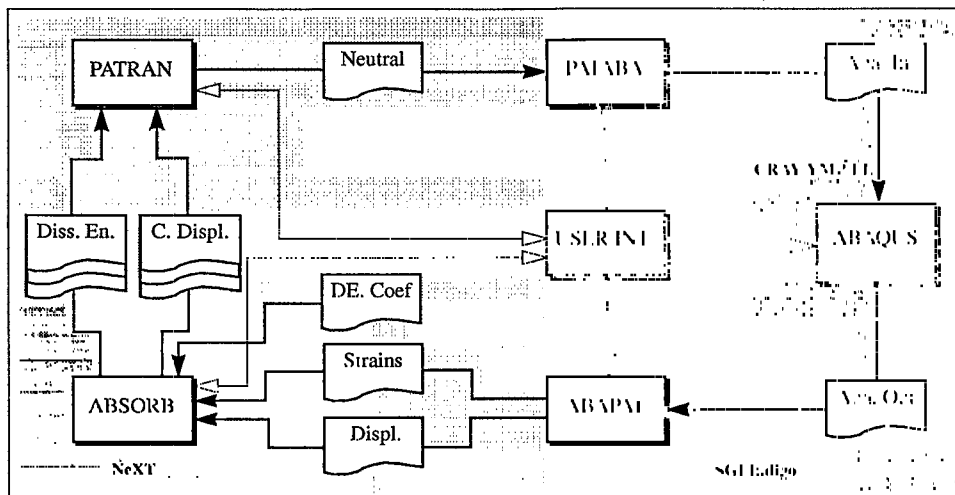


Fig. 1. Block diagram of the architecture of the structural simulator and computational resource allocation.

files to an “ABAQUS” input file. The output from “ABAQUS” is stored in a file that is subsequently converted to a strain file and a displacement file in “PATRAN” format by the “ABAPAT” process. The displacement files are identified by the suffix “.dis” and the strain files have the suffix “.els.” At this stage, the strains and displacements can be visualized from “PATRAN” or be fed into the dissipated energy module “ABSORB” which runs on a “NeXT” computer and generates a spatial energy absorption map by associating a value of dissipated energy with each strain combination at every spatial evaluation point. The required dissipated energy values are computed by interpolation using the coefficients in the file “rmt.x.y.pred” that were produced by the process depicted in Fig. 16 of Part I [6]. Finally, the white arrows that connect the user interface module with the other simulator modules signify user control over these modules through both the user interface and the networking TCP/IP utilities that control data transfer between the involved computing platforms.

There is currently an extensive effort at NRL to develop various simulating environments that can operate on stand alone computational architectures. Simplified versions with multimedia characteristics already exist for “MS-Windows 3.1” machines, and more advanced versions exist for the “SGI” platform.

3. Composite specimens

The specimen used in the IPL tests is an example of a structural object. It has structural loads, i.e., the loads applied by the IPL actuators. It has a structural geometry, i.e., the geometry of the specimen, and it has a structural material, i.e., the material under investigation. At any point within the structural object, strains are induced that act upon the material. In this instance, strains induced by the actuator loads act upon the specimen material. The strains are occasionally the same at different points of the specimen, but in general they are not. The strains act upon the specimen material, changing it on occasion. When

the strains do change, the material shows the change by exhibiting a different elastic behavior suggesting reduction in local stiffness (softening). The experimentally determined dissipated energy is a measure of material softening. It is a nonlinear, monotonic function of the strains that act upon the material. As such, the material exhibits behavioral changes that may be unexpected. This application uses the IPL structural object to showcase the nature of the unexpected behavior.

Consider material 002 in Table 1 that was used as the straw person in this application. With a layup construction of $[(+30/-30)_4]_s$, this laminated composite material has piles constructed from AS1 carbon fibers, and 3501-6 epoxy resin. Load icons were employed in the figures of this application to facilitate recognition of the particular load combination being applied to a specimen. Five graphic symbols were used in combination to produce these icons. They are: a clockwise arrow to indicate clockwise motion of the movable boundary of the specimen; a counterclockwise arrow to indicate the opposite motion; an upwards-pointing arrow to indicate motion of the points of the movable boundary parallel to the y -axis; a downwards arrow for the opposite motion; and a right-pointing arrow to indicate motion of the points of the movable boundary parallel to the x -axis.

The interpretation of a particular combination of the graphic symbols is that the corresponding combination of IPL applied motion is applied proportionally to the specimen's movable boundary. The specimen, caught between its movable and immovable boundaries, deforms with a compatible motion. Loads that are proportional to each other are represented by the same icon. The particular magnitude of the proportional load is indicated individually, or by group where applicable. That specimen dissipated energy is a continuous nonlinear monotonic function of load displacement magnitude is an experimentally determined fact. The material dissipation energy is forced to be a continuous nonlinear monotonic function of strain magnitude. Though the specimen, undeniably, is nonlinear monotonic, the computed material dissipation function behaves that way by analytic design.

Fig. 2 depicts the loading case for load path 11 (1p-11). The load magnitudes shown are 20, 40, and 60 percent of the maximum boundary motion applied during the experiment for this particular

specimen. Fig. 2 also illustrates the monotonic nature of dissipated energy with respect to strains. Dissipated energy never decreases with increasing magnitudes of loading. It is also apparent

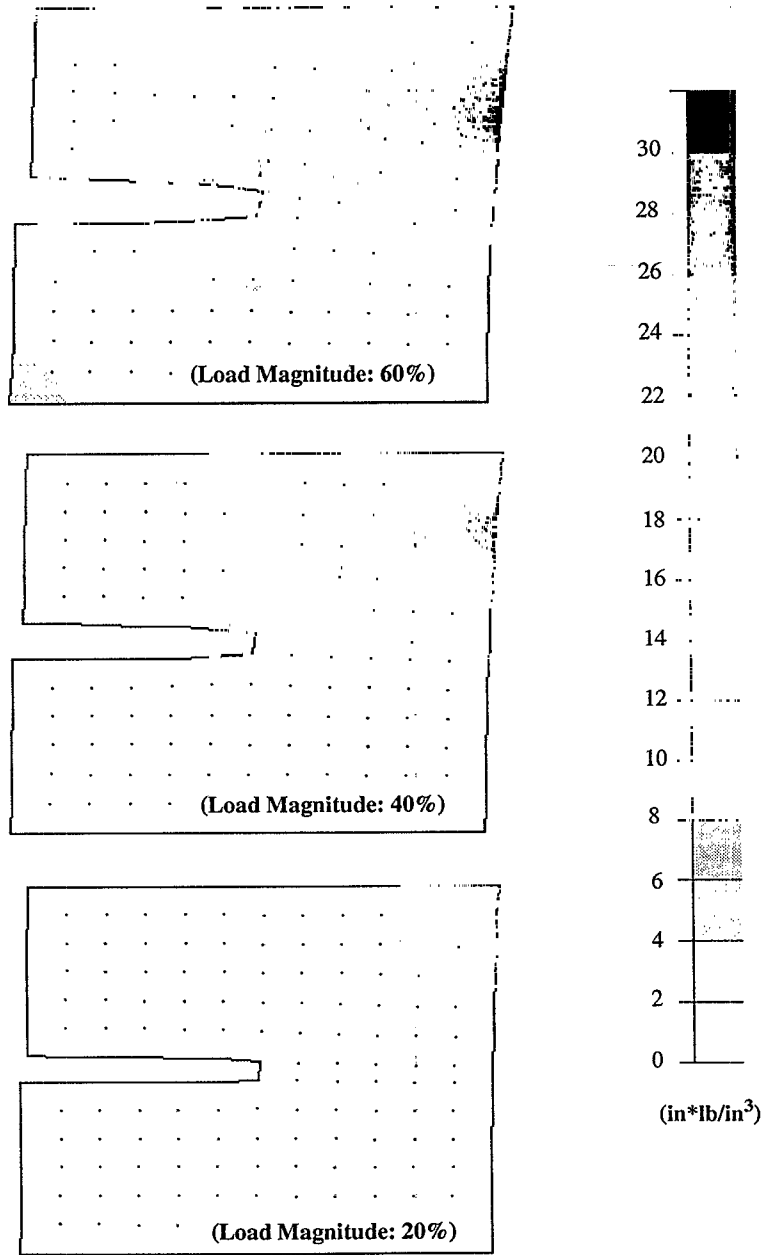


Fig. 2. Distributions of dissipated energy density on the deformed specimen for loading path 11, material 002 (AS1/3506-1 [$\pm 30^\circ$]) for three different magnitudes of loading.

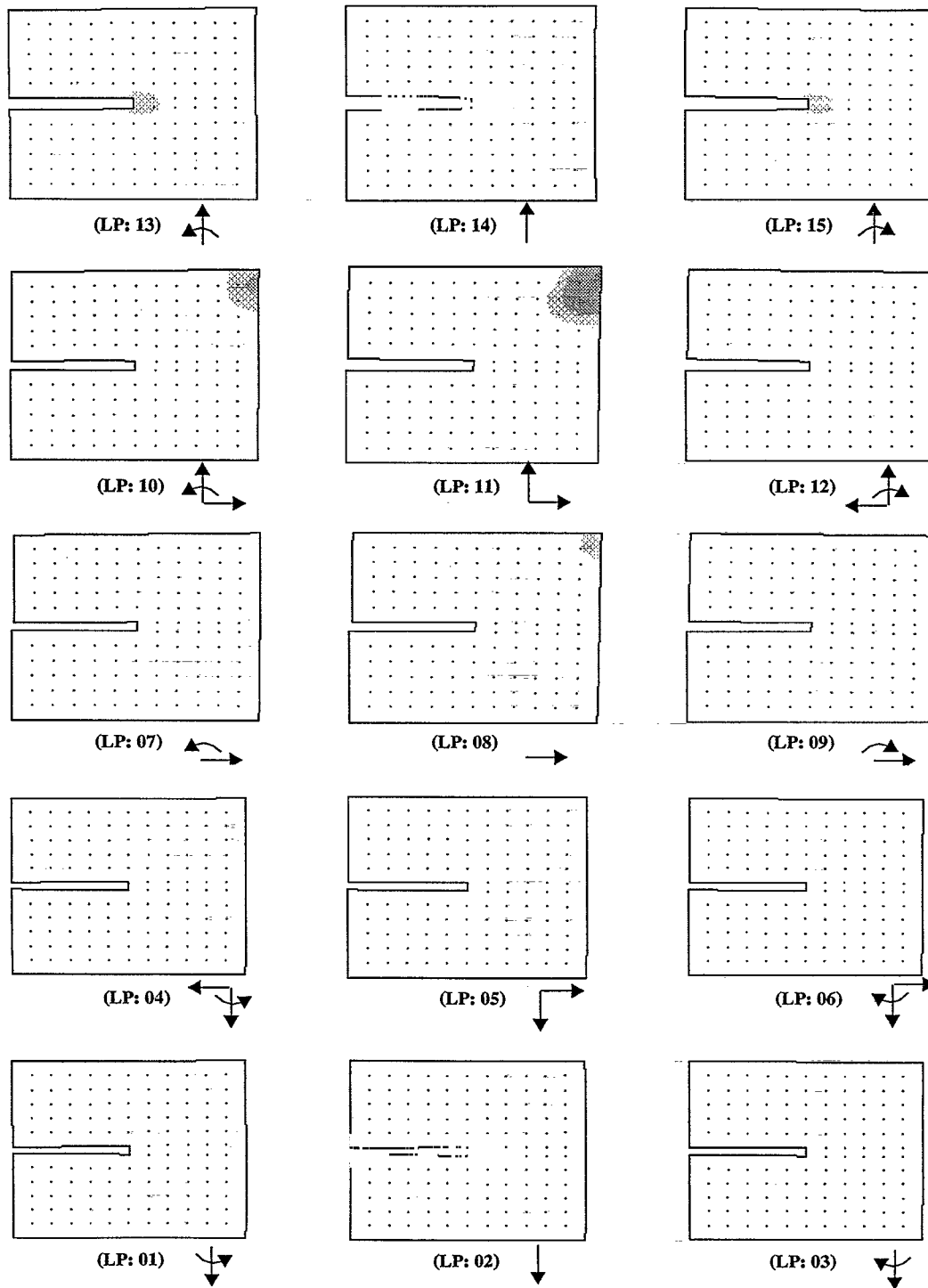


Fig. 3. Distributions of dissipated energy density on the deformed specimen for load magnitude 2, material 002 (AS1/3506-1 [$\pm 30^\circ$]), for each of the load paths 1–15.

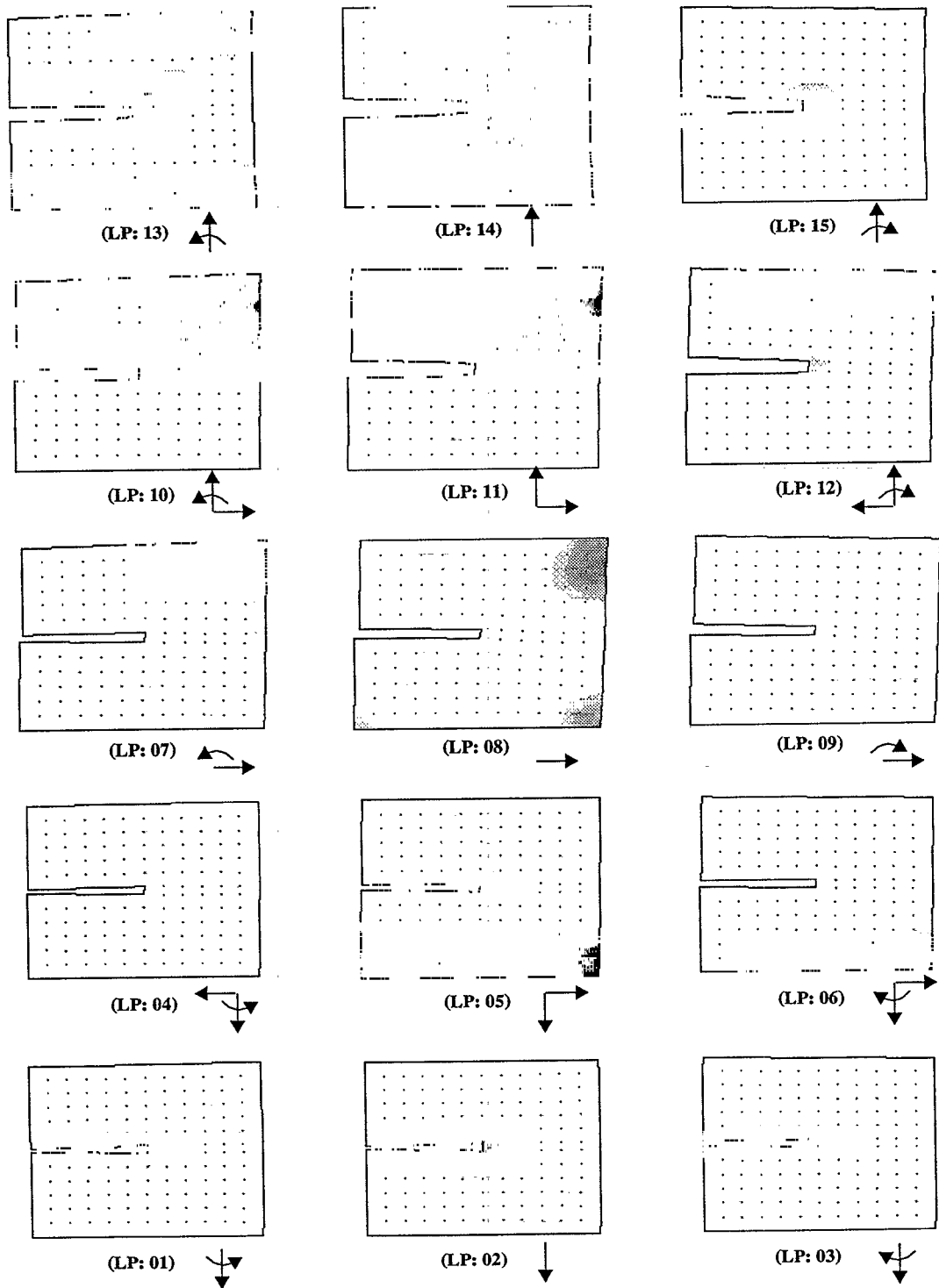


Fig. 4. Distributions of dissipated energy density on the deformed specimen for load magnitude 3, material 002 (AS1/3506-1 [$+/-30^\circ$]), for each of the load paths 1–15.

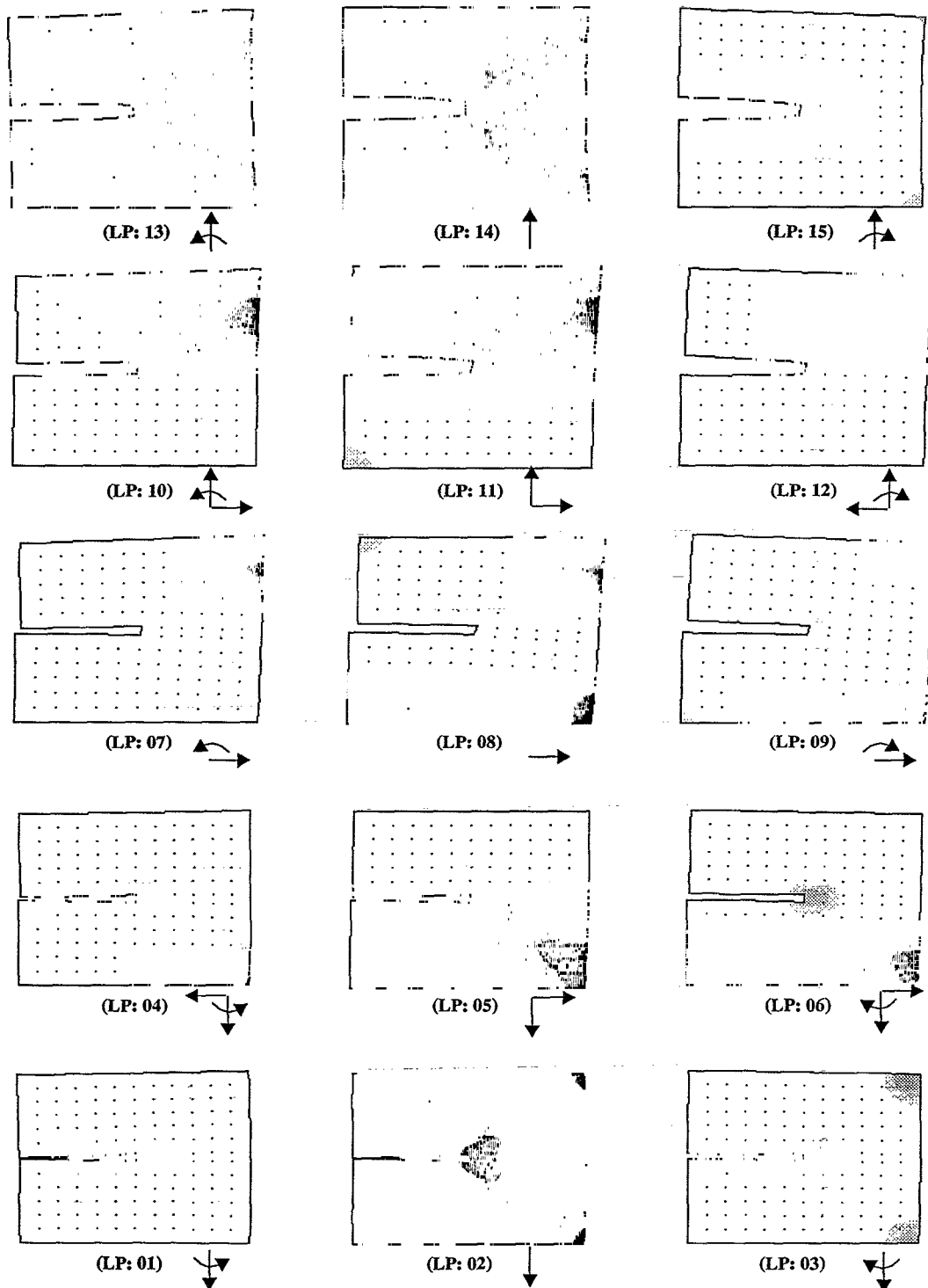


Fig. 5. Distributions of dissipated energy density on the deformed specimen for load magnitude 4, material 002 (AS1/3506-1 [$\pm 30^\circ$]), for each of the load paths 1-15.

here that the dissipated energy may not increase after reaching a certain magnitude of strain, and that a minimum magnitude of strain is required before the dissipated energy can become greater than zero. This observed behavior corresponds precisely to what is meant by the term a nonlinear monotonic function of strain magnitude.

To reiterate, that specimen dissipated energy is a continuous nonlinear function of load combination is an experimentally determined fact. In computing the material dissipation energy function from the specimen dissipated energy, the only analytic control exercised is to ensure continuous behavior with respect to the strain combination. Consequently, the nonlinear effect of strain combination as illustrated in Figs. 3, 4, and 5 is closely related to the experimentally observed behavior.

Figs. 3, 4, and 5 all depict the same set of the

15 different load combinations used in obtaining the experimental results. Fig. 3 is for the case of 20% of full load magnitude, while Fig. 4 is for 40%, and Fig. 5 for 60%. The effect of opening vs. closing motion (lp-14 vs. lp-2), which may be likened to tension vs. compression behavior, is quite distinctive. At the 20% level, both cases are indistinguishable. At the 40% load level, the opening or tension case has developed an extensive hot area from the notch tip out along the $\pm 30^\circ$ fiber directions all the way to the edge of the specimen, while the closing or compression case has changed only slightly. At the 60% load level, the situation has changed dramatically again. The compression case has developed a hot zone of the same configuration as that for tension. But while the zone for opening is diffuse, that for closing is concentrated at the notch and at the edge.

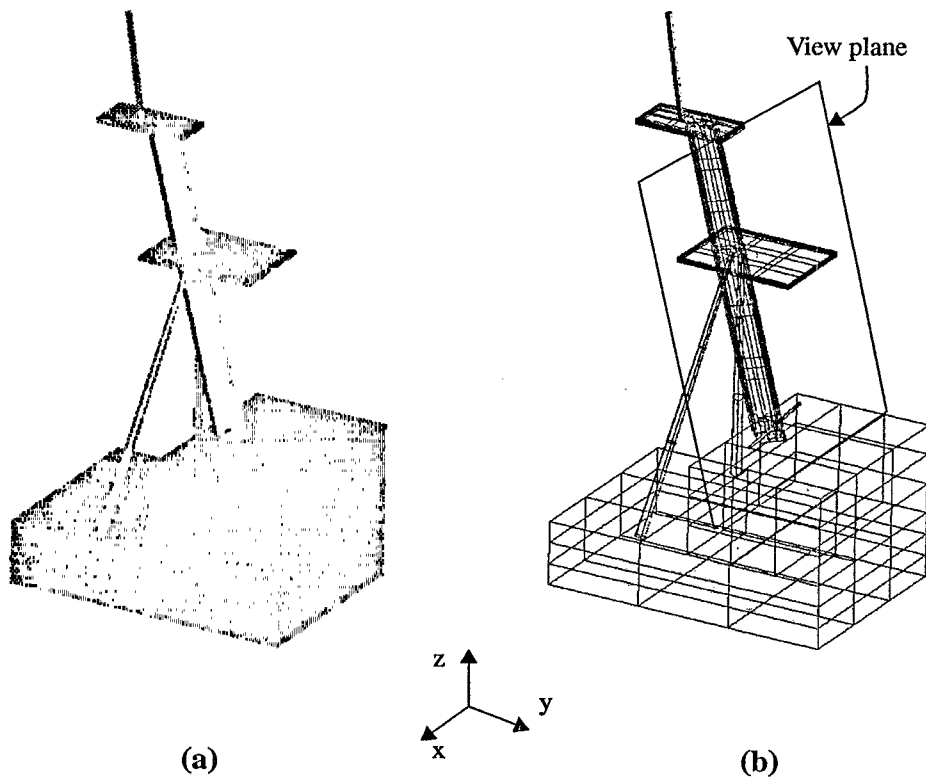


Fig. 6. Rendered view of (a) the mast structure and (b) wireframe view of the mast structure with the view plane used for displaying the dissipated energy density distributions.

The effect of opening, sliding, and closing load combinations (lp-14,lp-8,lp-2), demonstrates clearly the distinction between linear effect and nonlinear effect. The opening and sliding combinations is lp-11. Lp-14 and lp-8 both show extensive zones of nonzero dissipated energy in the lower half of the specimen. A linear effect would show dissipated energy as a proportional sum of the dissipated energy from cases lp-14 and lp-8. Clearly, lp-11 shows no nonzero dissipated energy in the lower half of the specimen. The effect is

typical of nonlinearity. The sliding, closing combination, lp-5, exhibits the same nonlinear effect.

The general assertion is that "if the IPL experiments were conducted using another specimen shape, then the material dissipation energy function would be the same". In other words, the material behavior should be independent of the structure or of the loads that may be applied to that structure. If the preceding discussion and Part I [6] had been about this alternative experimental specimen, then the different specimen

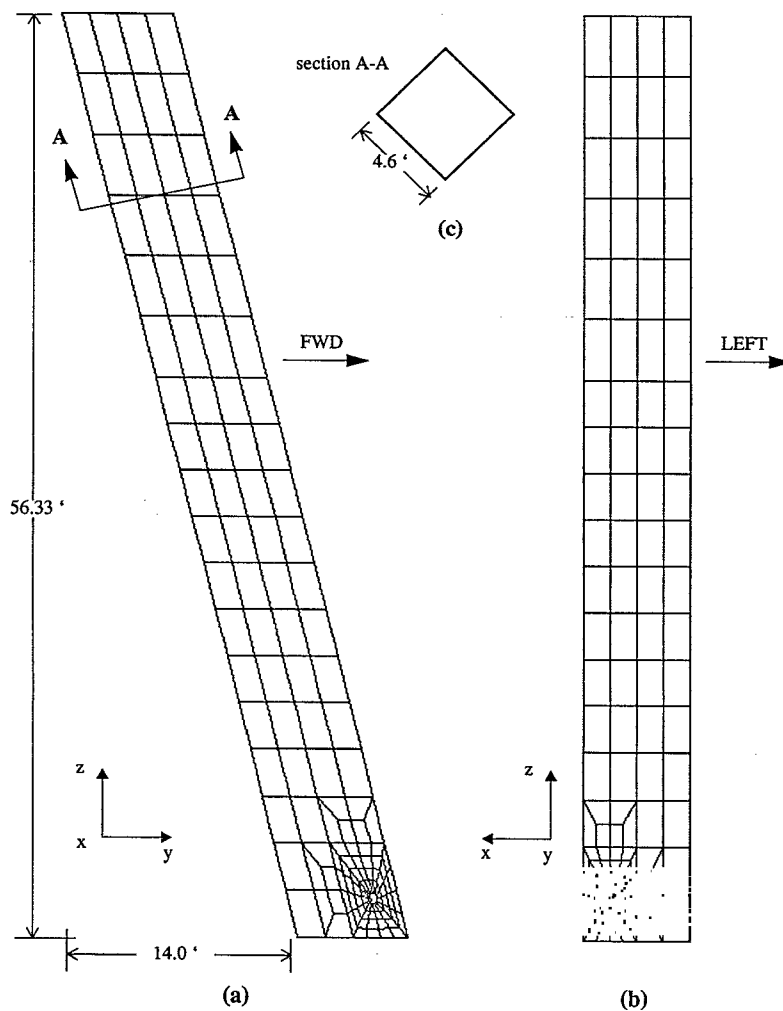


Fig. 7. Right side view of the finite element meshing and dimensions of the mast (a); front view of the mesh (b); cross section of the mast (c).

shape would have produced different strain distributions and consequently different material dissipated energy distributions. The same general continuous, nonlinear, monotonic nature of the material dissipation energy function would have been noted, but their distributions within the specimen would have been different. If a strong relationship had been drawn between the specimen, its loadings, and the consequent distributions of material dissipated energy from the cases presented, then a different strong relationship would have been drawn from consideration of the results for the alternative specimen.

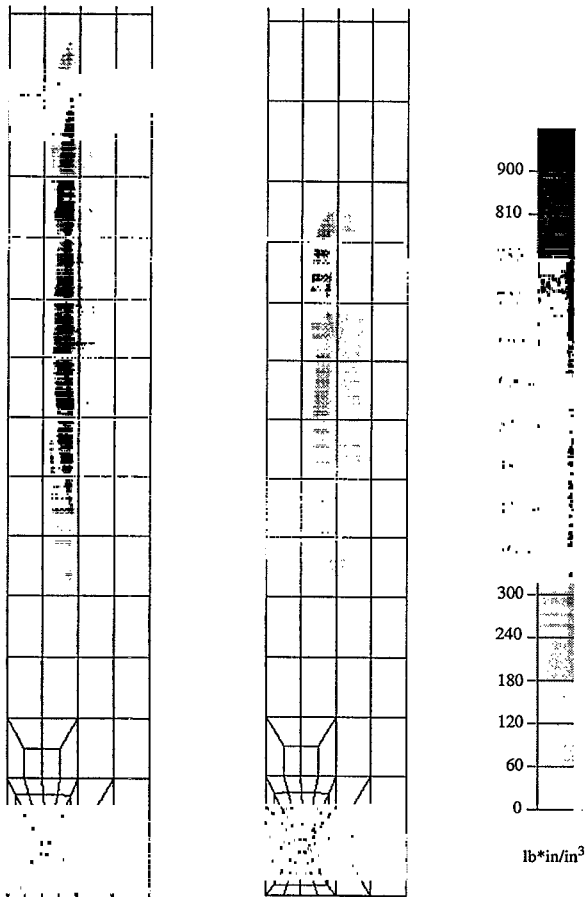


Fig. 8. Front views of dissipated energy density distributions of ship mast made out of thermoset material 007 (AS4/3501-6 [+/-60°]) (left) and out of thermoplastic material 040 (AS4/PEEK [+/-60°]) (right), for 1× the total loading corresponding of front wind.

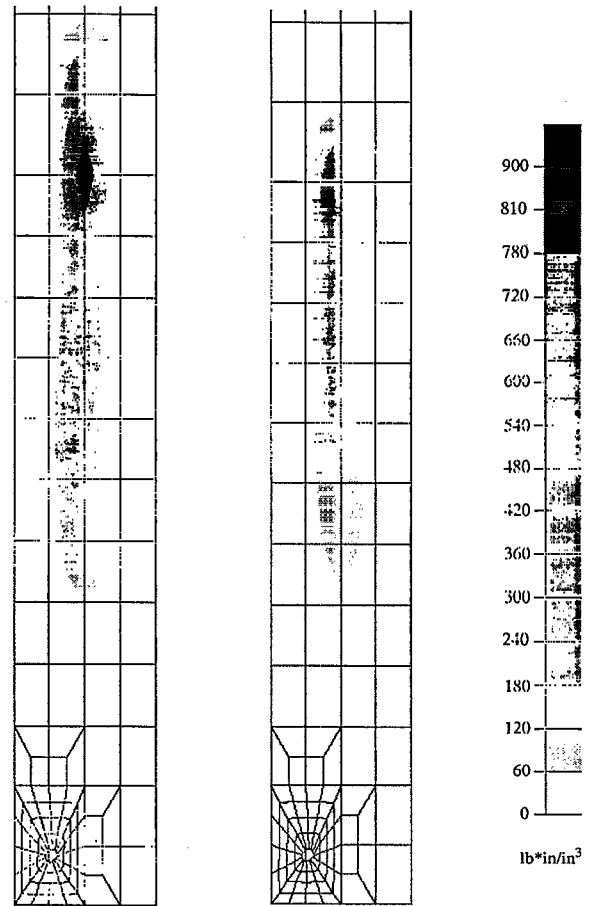


Fig. 9. Front views of dissipated energy density distributions of ship mast made out of thermoset material 007 (AS4/3501-6 [+/-60°]) (left) and out of thermoplastic material 040 (AS4/PEEK [+/-60°]) (right), for 2× the total loading corresponding of front wind.

The danger is in attempting to infer material behavior from specimen behavior, without regard to how the strains are distributed within that particular specimen.

4. Application to naval structures

Two specific naval structures have been chosen to demonstrate application of the dissipated energy density map distributions, to study effect of increasing loading and usage of different mate-

rials. These structures are a ship mast and an idealized submarine hull.

4.1. Ship mast

One of the design goals is to investigate the merits of using composite materials for ship masts. The primary reasons composite masts are being considered are weight reduction and favorable radar return characteristics. Traditional designs for metal masts were based on the assumption of linear elastic behavior and stress-based damage criteria; namely, that internal load-induced dam-

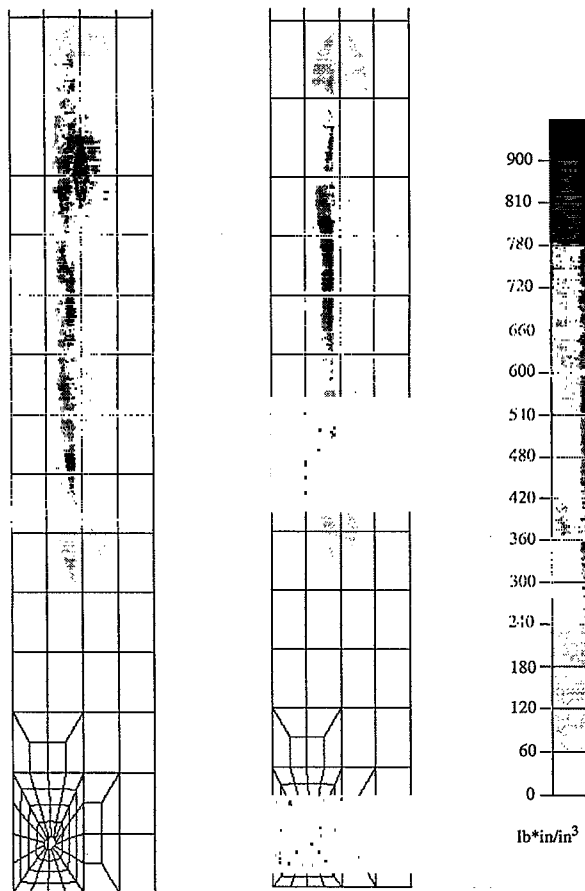


Fig. 10. Front views of dissipated energy density distributions of ship mast made out of thermoset material 007 (AS4/3501-6 [+/-60°]) (left) and out of thermoplastic material 040 (AS4/PEEK [+/-60°]) (right), for 3× the total loading corresponding to front wind.

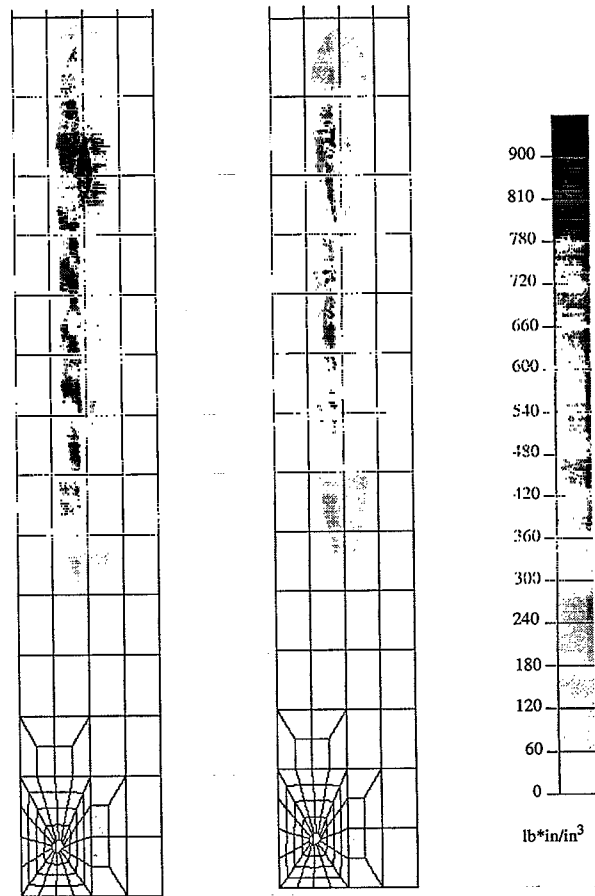


Fig. 11. Front views of dissipated energy density distributions of ship mast made out of thermoset material 007 (AS4/3501-6 [+/-60°]) (left) and out of thermoplastic material 040 (AS4/PEEK [+/-60°]) (right), for 4× the total loading corresponding to front wind.

age was assumed to occur whenever the stress exceeded a specified maximum stress set at 2.5 times the yield stress for the material used. As mentioned previously, such a simplistic view of failure behavior is not justified in composites, and a more realistic damage model such as the one being proposed in this study is required. The enhanced understanding provided by such a model should lead to lower safety factors and, therefore, more efficient mast designs. The structural response simulator together with a database of computed dissipated energy functions repre-

sent a unique medium to achieve the efficient design of composite masts.

The DDG-51 class of frigates was selected as a candidate ship for a representative mast installation. The geometry of the mast is that of a tripod mast with a rectangular box beam and two struts with two antenna platforms attached to it and the associated deckhouse as shown in Fig. 6. The design loads selected for this case were extracted from the “DDS-170” manual. For demonstration purposes, a wind load of 30 psf (lb/ft²) corresponding to a 90 kn head wind was selected. In addition, an inertial load of 0.6 g applied downwards to the center of gravity of the mast, or 0.2 g applied upwards on the center of gravity of the mast. A 500 lb antenna load was assumed to be applied at the upper platform and a 1000 lb antenna load applied at the lower platform of the mast were also considered. Only the case of head-on wind load is presented here, however.

The materials used for this simulation were item 007 (Resin 3501-6, Fiber AS4, Layup +/− 60°) and item 040 (Resin PEEK, Fiber AS4, Layup +/− 60°) as described in Table 1 of Part I [6]. These materials were selected to establish the relative merits of the thermoset 3501-6 resin material vs. the thermoplastic PEEK resin material. The material was composed of 130 successive

piles of 0.0075 in. each, thus accounting for a total thickness of 0.975 in. Fig. 7 shows the dimensions and the finite element mesh for the simulation of the mast structure itself. A total of 106 “ABAQUS” “QUAD” elements were used for the finite element idealization. In addition, battle damage was simulated by considering a 5 in. hole at the right side of the foot of the mast as shown in Fig. 7.

Figs. 8–11 present the simulation results for different loading and material choices as seen from the front of the mast in the region indicated in Fig. 6 with a rectangular window. All figures are fringe plots of the dissipated energy distribution over the structure. In all of these figures, the views on the left represent the dissipated energy distribution for the 3501-6 thermoset material, and the views on the right represent the dissipated energy distribution for the PEEK thermoplastic material.

The effect of applying an increasingly higher load corresponding to front wind is manifested as an increasingly higher distribution of fringes for higher levels of loading. Each one of these figures has been plotted for 1×, 2×, 3×, and 4× overload levels of the original 30 lb/ft² loading in the same order they appear in the document. Another characteristic of the response of the

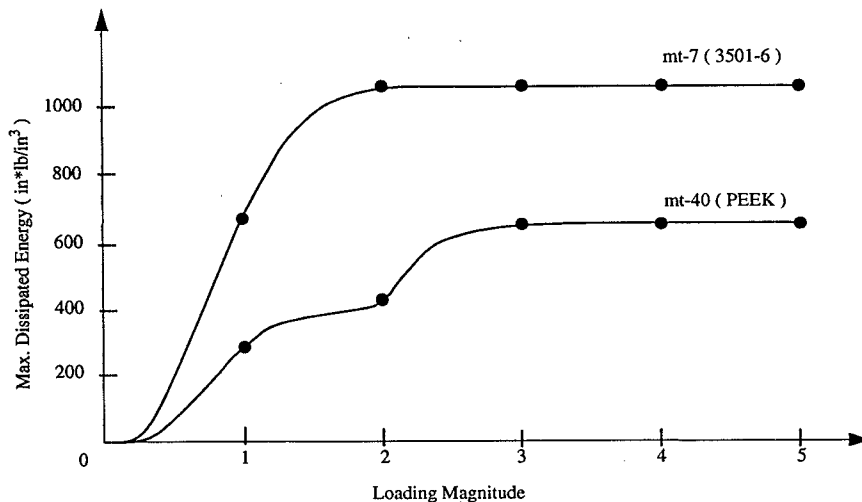


Fig. 12. Distribution of the maximum dissipated energy of the ship mast structure for materials 007 (AS4/3501-6 [+ / − 60°]) and 040 (AS4/PEEK [+ / − 60°]), vs. the loading magnitude.

structure due to the increasing load is the effect demonstrated in Fig. 12 where the maximum dissipated energy is plotted as a function of the load magnitude. That is, after a certain loading level, the material reaches a saturation level, where the dissipated energy in the material ceases to increase. This was the reason the distributions of overload magnitudes 4 and 5 were almost identical and, therefore, it seemed appropriate not to present the plotted distributions for loading magnitude 5. Evidence of this can be seen by comparing the dissipated energy distributions for loading magnitudes 3 and 4 in Figs. 8 and 11.

A significant observation is that the 3501-6 material seems to show a significantly higher propensity to go into its nonlinear region than does the PEEK material. This is evident from the higher number of fringes and their higher intensity as they appear on the 3501-6 distributions in Figs. 8–11 compared to those of the PEEK in Figs. 8–11. In addition, the 3501-6 material also has the tendency to dissipate higher amounts of dissipated energy as is shown by the saturation levels in Fig. 12. It is apparent from all these figures, that the mechanical damage, in terms of dissipated energy, caused by the round penetra-

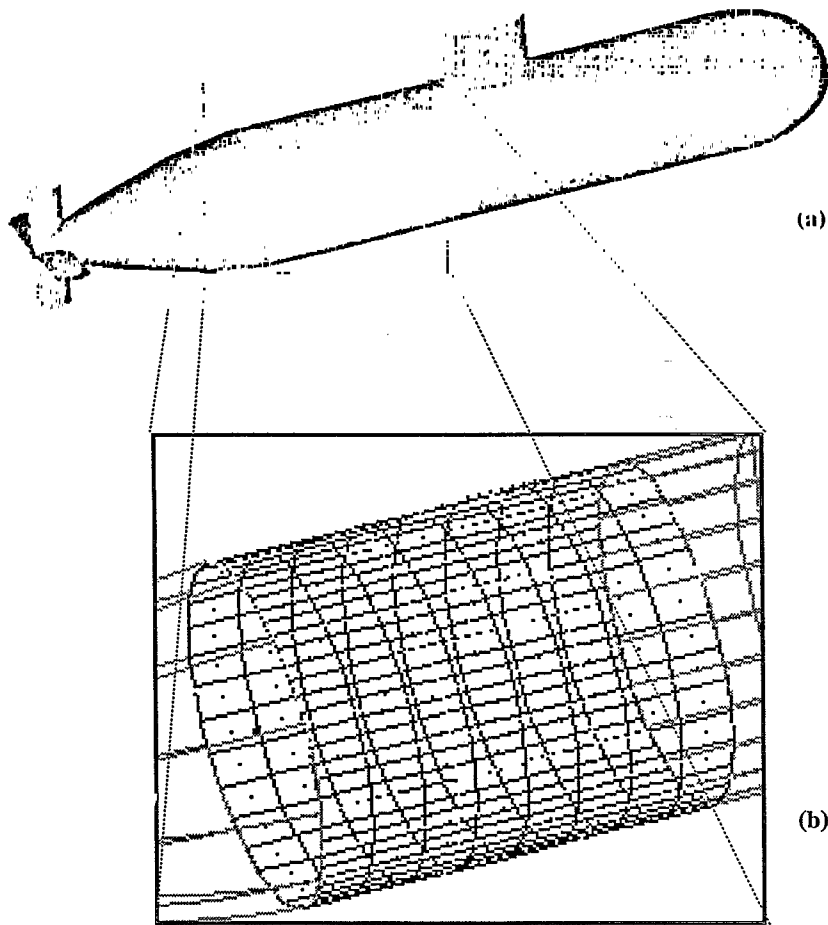


Fig. 13. Cylindrical shell as a section of (a) an idealized submarine, and (b) the corresponding finite element mesh.

tion on the left side of the base area of the mast is negligible compared to the one on the middle level of the structure.

4.2. Submarine Hull

An underwater structure, such as a submarine, is subject to a vast range of loads. These loads vary from underwater explosions, underwater wave actions, maneuvering loads, depth loads, to a whole variety of other types of loads. The survivability of the structure under these conditions is of prime importance. Since their invention, submarines have mainly been constructed from metals, but today, composites are being considered as a viable alternative. Dissipated en-

ergy offers a means of mapping out or hot spotting areas of concern on composite submarine structures. The structural loads, structural geometry, and the structural material act to produce strains throughout the structure that may induce changes in the material. Dissipated energy as a function of strain determines when a material will change from one elastic state to another, and is an important means of measuring both the extent of the material changes and the structural survivability.

Consider a generic submarine and, in particular, analyze the cylindrical hull section. The actual dimensions used are those of a generic dry dock shelter. The cylindrical shell idealization was selected as a simple showcase for dissipated

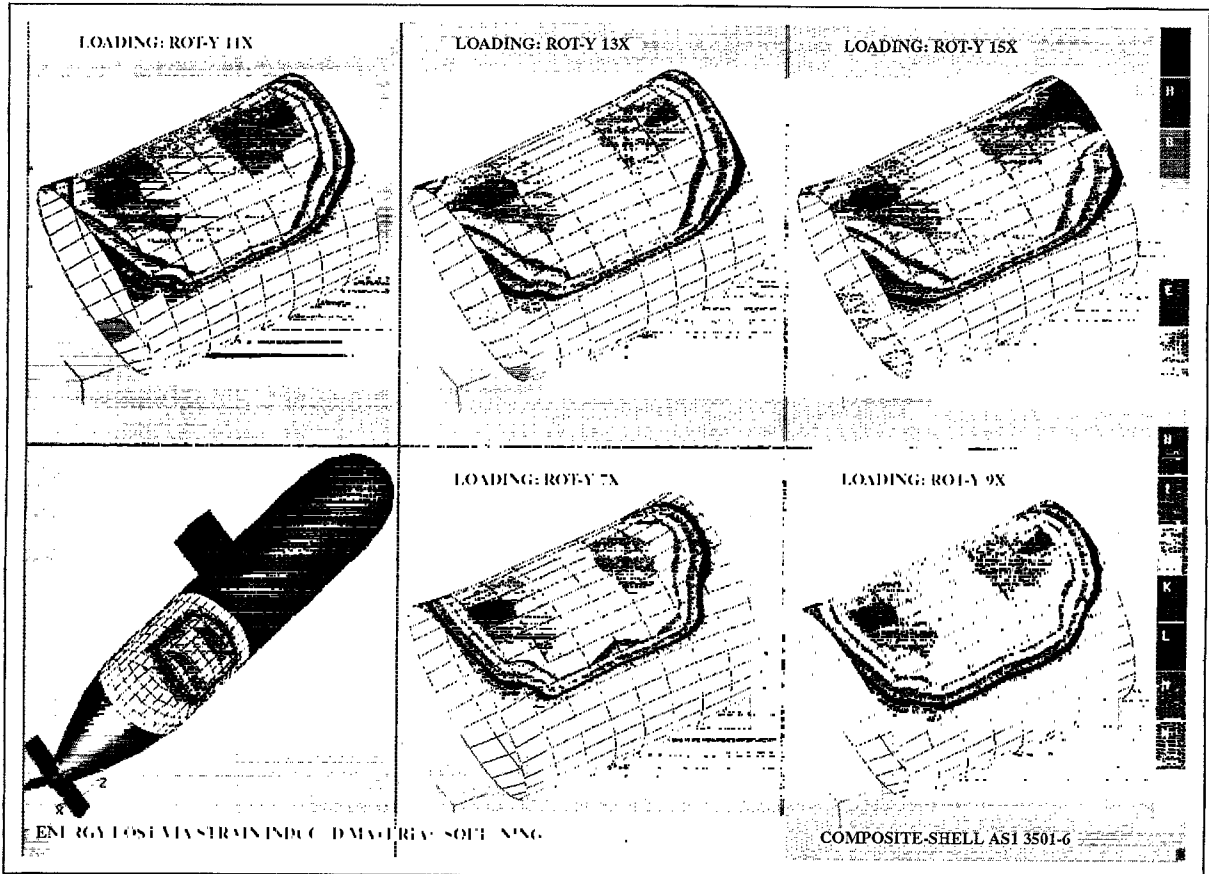


Fig. 14. Dissipated energy density distributions at the outer surface of the shell structure, for loading magnitudes of 7,9,11,13, and 15 times overload.

energy mapping. The finite element model used is shown in Fig. 13 and consists of 256 shell "QUAD" elements. The cylinder that was analyzed was 100 in. long, 80 in. diameter, and 1 in. thick. The boundary loading conditions were those induced by rigid body plane rotations of the ends of the cylinder. These loading conditions were chosen as a nominal representation of the kinds of loads that might be carried through to the cylinder by the rest of the submarine in response to bending loads about the vertical or y -axis. The shell material was a laminated graphite thermoset epoxy. The layers were oriented at $+/-60^\circ$ to the longitudinal, or z -axis. The fibers were AS4 and the resin was a 3501-6 type epoxy. The finite

element code "ABAQUS" was used to determine the interior strain field. The strains as reported back by the code are for the Gauss integration points used by "ABAQUS" to determine the shell properties. Three integration points were used in this analysis, one point at the center of the laminate and two points at about an eighth of the thickness in from each side. In this case, the dissipated energy is not computed on a per ply basis, but rather on a smeared-out point basis, or a partial dissipated energy number at an integration point. Gaussian integration is then used to compute a total dissipated energy through the thickness. Both types of dissipated energy are illustrated in the following figures where the par-

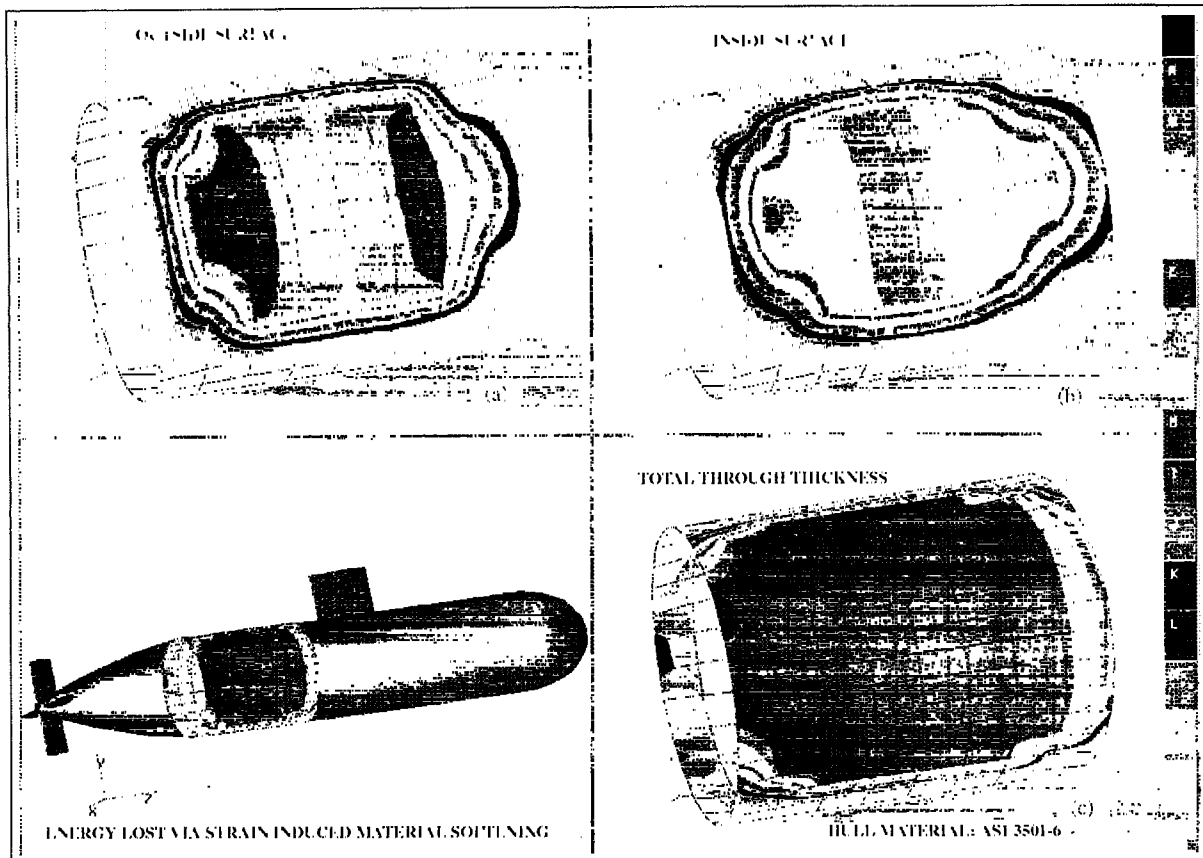


Fig. 15. Dissipated energy density distribution for (a) the inside surface of the shell, (b) the outside surface of the shell and (c) integrated through the thickness.

tial dissipated energy at the outer part of the shell is shown in Fig. 14 and total dissipated energy in Fig. 15.

Fig. 14 depicts the dissipated energy maps for overloads of 7X, 9X, 11X, 13X and 15X. The values shown are for partial dissipated energy close to the outer side of the shell. As can be seen in Fig. 14, the boundary of the hot-spotted zone (higher values of dissipated energy) at 7X overload is practically the same as at 15X overload. An observer may interpret this in several ways; however, it is reasonable to surmise that the damage as indicated by the hot-spotting is not going to grow unstably, and that regardless of the point of view taken as to the meaning of the damage, the material degrades only so far and thereafter gets no worse. Fig. 15 depicts the distribution of dissipated energy from below the inside surface, the outside surface, and throughout the thickness, i.e., partial vs. total viewpoints. The partial viewpoints show both similarities and differences. In both, the extent of the hot zone is roughly the same; however, each exhibits markedly different distributions within the zone.

The total dissipated energy viewpoint shows a larger hot zone than either of the partial dissipated energy maps. It also shows a rather constant value of dissipated energy over the area of the hot zone. From this an important inference may be drawn, that the nonlinear effect of strain on material loss of local stiffness, or change, may not be characterizable strictly on the basis of a partial or a total viewpoint.

5. Concluding remarks

The proposed procedure involves the determination of an energy density dissipation function which has the dimensions of energy per unit volume and is postulated to be a property of the material. Its volume integral equals the energy dissipated during loading because of the various internal failure events, and its value at any point in the material is regarded as a measure of load-induced internal damage. The energy dissipation function thus captures the collective behavior of these failure mechanisms without requiring an

explicit knowledge of these mechanisms, and, moreover, can also be related to local stiffness changes that lead to a form of nonlinear structural behavior. Determined are the energy dissipation function from data obtained by means of an extensive series of tests performed with NRL's In-Plane Loader, which is a computer-controlled testing machine capable of producing multiple combinations of opening/closing, sliding, and rotating boundary displacements.

Application of the method makes use of a computational approach packaged as a material response simulator that simulates the structural response of several structures of interest. These are the test specimen itself, a ship's mast, and a cylindrical shell representing an idealized section of a submarine hull. A number of different composite material systems are considered and spatial maps of the dissipation function (softening maps) are produced for various loading magnitudes. These softening maps illustrate how the energy consumed by the various internal failure events is dissipated within the structure.

Acknowledgements

The authors wish to acknowledge past and current financial support of the following Navy organizations and the indicated program managers:

Office of Naval Technology (J.J. Kelly³ and I.L. Caplan³ (DTRC Block Manager); Strategic Systems Project Office (E.L. Throckmorton³, R. Kinert, and F. Vondersmith); Naval Air Systems Command (C.F. Bersch); Naval Sea Systems Command (H.H. Vanderveldt, C. Zanis, W.R. Graner, and T.F. White).

The authors also wish to acknowledge helpful technical discussions with H. Marshall, Lockheed Palo Alto Research Laboratory, and J. Pitman, Gibbs and Cox Inc.

³ Current Program Managers.

References

- [1] R. Badaliance and H.D. Hill, Damage mechanisms and life prediction of graphite/epoxy composites, in: *STP775 Damage in Composite Materials*, ed. K.L. Reifsnider (ASTM, Philadelphia, PA, 1982) pp. 229–242.
- [2] J.E. Masters and K.L. Reifsnider, An investigation of cumulative damage development in quasi-iso-tropic graphite/epoxy, in: *STP775 Damage in Composite Materials*, ed. K.L. Reifsnider (ASTM, Philadelphia, PA, 1982) pp. 40–62.
- [3] A. Highsmith and K.L. Reifsnider, Stiffness-reduction mechanisms in composite laminates, in: *STP775 Damage in Composite Materials*, ed. K.L. Reifsnider (ASTM, Philadelphia, PA, 1982) pp. 103–117.
- [4] G.C. Sih, Impact damage of laminated composites with energy dissipation: Part I. Nonhomogeneous characteristics, *J. Theoret. and Appl. Fract. Mech.* 22, No. 3, to be published.
- [5] G.C. Sih, Impact damage of laminated composites with energy dissipation: Part II. damage evolution, *J. Theor. and Appl. Fract. Mech.* 22, No. 3, to be published.
- [6] P.W. Mast, G.E. Nash, J.G. Michopoulos, R. Thomas, R. Badaliance and I. Wolock, Characterization of strain-induced damage in composites based on the dissipated energy density: Part I. Basic scheme and information, this issue *J. Theor. and Appl. Fract. Mech.* 22, 71–96 (1995).
- [7] J.G. Michopoulos, G.C. Sih, S.C. Chou and J.F. Dignam, Energy dissipation in highly compressed cylindrical bar specimens, *J. Theoret. and Appl. Fract. Mech.* 2, 105–110 (1984).
- [8] G.C. Sih, Thermal/Mechanical Interaction Associated with the Micromechanisms of Material Behavior, Institute of Fracture and Solid Mechanics, Lehigh University, Bethlehem, PA (1987).
- [9] G.C. Sih, D.Y. Tzou and J.G. Michopoulos, Secondary temperature fluctuation in cracked 1020 steel specimen loaded monotonically, *J. Theoret. and Appl. Fracture Mech.* 7, 74–87 (1987).
- [10] E.T. Onat and F.A. Leckie, Representation of mechanical behavior in the presence of changing internal structure, *J. Appl. Mech.* 55, 1 (1988).

THEORETICAL AND APPLIED FRACTURE MECHANICS

Aims and Scope

Mechanics and Physics of Fracture

The "Mechanics and Physics of Fracture" portion encourages publication of original research on material damage leading to crack growth and/or fatigue. Materials treated include metal alloys, polymers, composites, rocks, ceramics, etc. The material damage process is complex because it involves the combined effect of loading, size and geometry, temperature and environment. Formulation may involve the dissipation of energy in various forms and the identification of microscopic entities and their interactions with macroscopic variables. The advent of the modern computer, however, has offered added capability for analyzing the stresses and/or strains and failure modes. The construction and verification of quantitative theories can be more readily carried out. Encouraged in particular are contributions related to predictions of material damage behavior based on microscopic and/or macroscopic models.

Aims and Scope

Fracture Mechanics Technology

The "Fracture Mechanics Technology" section emphasizes material characterization techniques and translation of specimen data to design. Contributions shall cover the application of fracture mechanics to hydro and electric machineries, off-shore oil exploration equipments, pipelines and pressure vessels, nuclear reactor components, air, land and sea vehicles, and many others. Among the areas to be emphasized are:

- Case Histories
- Material Selection and Structure Design
- Sample Calculations of Practical Design Problems
- Material Characterization Procedures
- Fatigue Crack Growth and Corrosion
- Nondestructive Testing and Inspection
- Code Requirements and Standards
- Structural Failure and Aging
- Failure Prevention Methodologies
- Maintenance and Repair
- Product Liability and Technical Insurance

Subscription Information

THEORETICAL AND APPLIED FRACTURE MECHANICS (ISSN 0167-8442). For 1994 volumes 21-22 are scheduled for publication.

Subscription prices are available upon request from the publisher. Subscriptions are accepted on a prepaid basis only and are entered on a calendar year basis. Issues are sent by surface mail except to the following countries where air delivery via SAL mail is ensured: Argentina, Australia, Brazil, Canada, China, Hong Kong, India, Israel, Japan, Malaysia, Mexico, New Zealand, Pakistan, Singapore, South Africa, South Korea, Taiwan, Thailand, USA. For all other countries airmail rates are available upon request.

Claims for missing issues must be made within six months of our publication (mailing) date.

Please address all your requests regarding orders and subscription queries to: Elsevier Science, Journals Department, P.O. Box 211, 1000 AE Amsterdam, The Netherlands. Tel.: 31-20-4853642, FAX: 31-20-4853598.

Information for Contributors

Manuscripts in English should be submitted in triplicate to the Editor-in-Chief or communicated via a member of the Board of Editors who is most closely associated with the content of the work. In the latter case, one copy of the manuscript should be sent to the office of the Editor-in-Chief.

Upon acceptance of an article, author(s) resident in the USA will be asked to transfer copyright of the article to the publisher. This transfer will ensure the widest possible dissemination of information under the U.S. Copyright Law.

There are no page charges. Cost for alterations in proofs other than printer's errors will, however, be charged to the authors.

Fifty reprints of each paper will be provided free of charge. Additional reprints can be ordered at cost.

The language of the manuscript should be in English. Manuscripts submitted in other languages may be considered at the discretion of the Board of Editors.

Manuscripts should be typed double spaced on one side of the page only with wide margins. The first page of the manuscript should contain: a title, name(s) of author(s), affiliation(s), and a short abstract.

All mathematical symbols which are not typewritten should be specified and listed separately. Unusual symbols or notations should be identified in the margins. Awkward mathematical notations which require special typesetting procedures must be avoided. The numbers identifying displayed mathematical expressions should be placed in parentheses. The use of metric units of the SI (Système Internationale) form is obligatory.

Illustrations are to be restricted to the minimum necessary. Originally drawn figures and glossy prints of photographs should be provided in a form suitable for photographic reproduction and reduction. Each figure should have a number and a caption; the captions should be collected on a separate sheet. The appropriate place of a figure should be indicated in the margin.

References to published literature should be quoted in the text in square brackets and grouped together at the end of the paper in numerical order. Journal titles should be abbreviated in the style of the 4th edition of the World List of Scientific Periodicals, and references should be arranged as

[1] L.F. Gillemot, Criterion of crack initiation and spreading, *J. Eng. Fract. Mech.* 8, 239-253 (1976).

for Journal articles and

[2] N.I. Muskhelishvili, *Some Basic Problems of the Mathematical Theory of Elasticity*, Second English ed., (Noordhoff: Groningen, Netherlands, 1963).

for books.

ELSEVIER SCIENCE

prefers the submission of electronic manuscripts

Electronic manuscripts have the advantage that there is no need for the rekeying of text, thereby avoiding the possibility of introducing errors and resulting in reliable and fast delivery of proofs.



The preferred storage medium is a 5.25 or 3.5 inch disk in MS-DOS format, although other systems are welcome, e.g. Macintosh.



After **final acceptance**, your disk plus one final, printed and exactly matching version (as a printout) should be submitted together to the accepting editor. **It is important that the file on disk and the printout are identical.** Both will then be forwarded by the editor to Elsevier.



Please follow the general instructions on style/arrangement and, in particular, the reference style of this journal as given in "Instructions to Authors."



Please label the disk with your name, the software & hardware used and the name of the file to be processed.



THEORETICAL AND APPLIED FRACTURE MECHANICS

Please send me a free sample copy

Please send me subscription information

Please send me Instructions to Authors

Name _____

Address _____



ELSEVIER
SCIENCE

Send this coupon or a photocopy to:

ELSEVIER SCIENCE B.V

Attn: Engineering and Technology Department
P.O. Box 1991, 100 BZ Amsterdam, The Netherlands

Reprinted from

theoretical and applied fracture mechanics

fracture mechanics technology

Theoretical and Applied Fracture Mechanics 22 (1995) 97-114

Characterization of strain-induced damage in composites based
on the dissipated energy density

Part II. Composite specimens and naval structures

P.W. Mast, G.E. Nash ¹, J.G. Michopoulos ^{*}, R. Thomas ², R. Badaliane, I. Wolock [†]

*Mechanics of Materials Branch, Materials Science and Technology Division, U.S. Naval Research Laboratory,
Washington, DC 20375, USA*



THEORETICAL AND APPLIED FRACTURE MECHANICS

Editor-in-Chief

G.C. Sih, *Institute of Fracture and Solid Mechanics, Lehigh University, Bethlehem, PA 18015, USA*

Board of Editors

Fracture Mechanics Technology

N.N. Au, *USA*
J.T. Barnby, *UK*
C.M. Branco, *Portugal*
A. Carpinteri, *Italy*
C.I. Chang, *USA*
S.C. Chou, *USA*
D. Corderoy, *Australia*
A. DiTommaso, *Italy*
M. Elices, *Spain*
K.F. Fischer, *Germany*
G.G. Garrett, *South Africa*

E.E. Gdoutos, *Greece*
F. Gillemot, *Hungary*
D.P.H. Hasselman, *USA*
A.R. Ingraffea, *USA*
R. Jones, *Australia*
H.-W. Liu, *USA*
S.N. Monteiro, *Brazil*
O. Orringer, *USA*
J.C. Radon, *UK*
C.W. Smith, *USA*

Mechanics and Physics of Fracture

G.I. Barenblatt, *Russia*
G. Caglioti, *Italy*
E. Kröner, *Germany*
S.T. Mileiko, *Russia*
H. Mughrabi, *Germany*
J.T. Pindera, *Canada*
J.W. Provan, *Canada*
E. Sommer, *Germany*
M. Sokolowski, *Poland*
V. Tamuzs, *Latvia*

© 1995, Elsevier Science B.V. All rights reserved.

No part of this publication may be reproduced, stored in a retrieval system or transmitted in any form or by any means, electronic, mechanical, photocopying, recording or otherwise, without the prior permission of the publisher, Copyright & Permissions Department, Elsevier Science B.V., P.O. Box 521, 1000 AM Amsterdam, The Netherlands.

Special regulations for authors – Upon acceptance of an article by the journal, the author(s) will be asked to transfer copyright of the article to the publisher. This transfer will ensure the widest possible dissemination of information.

Special regulations for readers in the U.S.A. – This journal has been registered with the Copyright Clearance Center, Inc. Consent is given for copying of articles for personal or internal use, or for the personal use of specific clients. This consent is given on the condition that the copier pays through the Center the per-copy fee stated in the code on the first page of each article for copying beyond that permitted by Sections 107 or 108 of the U.S. Copyright Law. The appropriate fee should be forwarded with a copy of the first page of the article to the Copyright Clearance Center, Inc., 222 Rosewood Drive, Danvers, MA 01923, U.S.A. If no code appears in an article, the author has not given broad consent to copy and permission to copy must be obtained directly from the author. The fee indicated on the first page of an article in this issue will apply retroactively to all articles published in the journal, regardless of the year of publication. This consent does not extend to other kinds of copying, such as for general distribution, resale, advertising and promotion purpose, or for creating new collective works. Special written permission must be obtained from the publisher for such copying.

USA mailing notice – Theoretical and Applied Fracture Mechanics (ISSN 0167-8442) is published six times per year by Elsevier Science, Molenwerf 1, P.O. Box 211, 1000 AE Amsterdam, The Netherlands. The annual subscription price in the USA is US\$ 475 (valid in North, Central and South America only), including air speed delivery. Second class postage is paid at Jamaica, NY 11431.

USA POSTMASTERS: Send address changes to Theoretical and Applied Fracture Mechanics, Publications Expediting, Inc., 200 Meacham Avenue, Elmont, NY 11003. Airfreight and mailing in the USA by Publications Expediting.

No responsibility is assumed by the Publisher for any injury and/or damage to persons or property as a matter or products liability, negligence or otherwise, or from any use or operation of any methods, products, instructions or ideas contained in the material herein. Although all advertising material is expected to conform to ethical standards, inclusion in this publication does not constitute a guarantee or endorsement of the quality or value of such product or of the claims made of it by its manufacturer.

∞ The paper used in this publication meets the requirements of ANSI/NISO 239.48-1992 (Permanence of Paper).

Published bi-monthly

0167-8442/95/\$09.50

Printed in The Netherlands



Characterization of strain-induced damage in composites based on the dissipated energy density

Part II. Composite specimens and naval structures

P.W. Mast, G.E. Nash ¹, J.G. Michopoulos ^{*}, R. Thomas ², R. Badaliane, I. Wolock [†]

Mechanics of Materials Branch, Materials Science and Technology Division, U.S. Naval Research Laboratory, Washington, DC 20375, USA

Abstract

Completed in Part I of this work are the description of the basic scheme and formulation by characterizing the damage behavior of composites by application of the dissipated energy density. Part II presents the development of a structural response simulator tool for composite structures subjected to different combinations of boundary displacements and loads. A presentation of distributions of dissipated energy density for the different load combinations on the specimens used in the In-Plane Loader (IPL) procedure described in Part I follows. Simulated response for several structures of interest to the Navy is also presented. They include a ship's mast and a cylindrical shell representing an idealized section of a submarine hull. Displayed are spatial maps of the dissipated energy density (softening maps) for various loading amplitudes. These softening maps reflect how energy is consumed by the different failure events within the structure.

1. Introduction

The use of composite materials in structural components has increased dramatically in recent years as their cost of production continues to decline and advances in composite design methodology become increasingly wide spread. As applications become more demanding, the need for reliable prediction of their mechanical

properties and behavior is becoming ever more important.

Extensive efforts have been made [1-5] in recent years to identify the various modes of damage in composite materials. Also refer to the references in Part I [6]. The primary finding of most of these investigations was that macroscopic fracture was usually preceded by an accumulation of the different types of microscopic damage and occurred by the coalescence of this small-scale damage into macroscopic cracks. Additionally, it was generally found that analyses based on classical fracture mechanics did not adequately model the damage effects and did not provide a satisfactory degree of predictive capability.

A more practical approach to modeling failure

^{*} Corresponding author. E-mail yiannis@prologos.nrl.navy.mil.

¹ Retired.

² Presently with FMT.

[†] Deceased

behavior in composites is to quantify the damage development on a continuum basis and relate it to the material constitutive behavior. The goal of such an approach is to permit accurate modeling of the progressive loss of stiffness and concomitant inelastic behavior caused by the underlying micromechanisms of damage [7–10]. Such a model for composite failure behavior requires a large parameter space for its description if it is to represent physical fact in a high-fidelity, objective manner. The model must be generic and phenomenological in nature and must rely on extensive sets of experimental data to identify the model parameters. Only after these parameters are determined can the model be related to particular failure mechanisms.

Following the basic scheme and formulation developed Part I [6] for relating the dissipated energy density as a function of strain in terms of a set of known basis functions and a set of undetermined coefficients. The task is then to estimate these coefficients. To accomplish this, a number of test specimens are first subjected to a range of prescribed combinations of in-plane loads using the In-Plane Loader [6]. These loads induce a wide range of internal strain states in the specimens. These states approximately encompass those expected in typical structural components under service loading conditions. The boundary displacements and boundary loads are measured for each load combination, and are used to compute the energy dissipated internally in the specimens caused by strain-induced damage for each test. The strain fields associated with each of the load combinations are also determined by means of a linear finite element analysis using the constitutive properties of the undamaged (virgin) material. The computation, therefore, neglects the effects of stiffness changes induced by the internal damage, but should be sufficiently accurate provided that no large-scale stress redistribution occurs during the tests. Analytic estimates of the dissipated energy are then computed in terms of the unknown coefficients for each test using the representation of the dissipation function, the computed strain fields, and the fact that the volume integral of the dissipation function equals the dissipated energy.

Finally, the undetermined coefficients in the dissipation function representation are determined by minimizing the difference between the experimentally measured and the analytic estimates of the dissipated energy for all the tests.

The aforementioned procedure is a deconvolution procedure in the sense that the goal is to extract a material property (the dissipated energy density function) from information obtained from the material in a particular physical configuration, namely the specimen, and, thus, it is necessary to factor out specimen geometry effects. By taking this approach, the resulting dissipated energy density function can be applied to any structural configuration, and used to develop material softening (stiffness reduction) maps for any structure (again, assuming a negligible amount of stress redistribution caused by internal damage).

Applicability of the model is demonstrated by describing a computational approach packaged as a material response simulator and its use in simulating the structural response of several structures of interest. These are the test specimen itself, a ship's mast, and a cylindrical shell representing an idealized section of a submarine hull. A number of different composite material systems are considered and spatial maps of the dissipation function (softening maps) are produced for various loading magnitudes. These softening maps illustrate how the energy consumed by the various internal failure events is dissipated within the structure.

2. Structural response simulator

The idea of a structural response simulator will be developed and it will be shown how the computed energy dissipation functions can be used within the simulator to design structural components and predict various aspects of their mechanical behavior. Because dissipated energy is taken as a measure of internal structural damage, one use of a simulator would be for structural designers to examine simulated spatial dissipated energy distributions to form selection criteria for evaluating the structural response of structures at a particular state of the design process.

Material system designers could also use a simulator to generate spatial dissipated energy maps from which they could determine the material response of a composite material system, and then select sets of manufacturing parameters to optimize the damage tolerance of new systems. Using the simulator to analyze material softening distribution patterns could also assist in selecting a material system for a particular structural design. Finally, a structural response simulator could even be used to qualify material systems by using far more realistic qualification criteria than are currently employed, e.g., strength or fracture toughness, which only indirectly and partially assess some qualitative aspects of the materials. Indeed, it is shown in this section that higher strength does not necessarily imply better damage tolerance.

In order to develop a tool for addressing the types of problems discussed above, a structural response simulator was created that takes user-specified geometries, materials, and loading conditions as inputs and creates spatial material distributions of local stiffness loss using the experimentally obtained dissipated energy functions. Fig. 1 shows the architecture of the structural response simulator in the configuration used to generate the results presented in this section. It has since evolved into a much more sophisticated

form and its design now includes such advanced functionality as user-simulator interaction modelling via artificial neural nets and other techniques.

The Fig. 1 block diagram shows the structure of the simulator in terms of component subsystems. The user interface was created by writing a library of function calls using the "PATRAN Command Language" (PCL) that allows the user to specify the geometry, the material, and the loading for the structure of interest. Visualization capabilities are provided through PDA's "PATRAN" 2.4 solid modeling package. A finite element idealization of the structure is achieved through appropriate use of PCL and all relevant model information is stored in "PATRAN" neutral files on the mass storage memory resources of the computer system hosting the simulator, which is currently a "Silicon Graphics Indigo" with 32 Mb of RAM and 2.5 GB of mass storage memory. The actual finite element analysis is performed by using the "ABAQUS" finite element code on a CRAY YMP/EL mini supercomputer, and assuming linear elastic behavior. The objective of the finite element analysis is to generate the strain field in the structure for the initial elastic state. The data required by "ABAQUS" are provided by the "PATABA" process that translates the "PATRAN" neutral

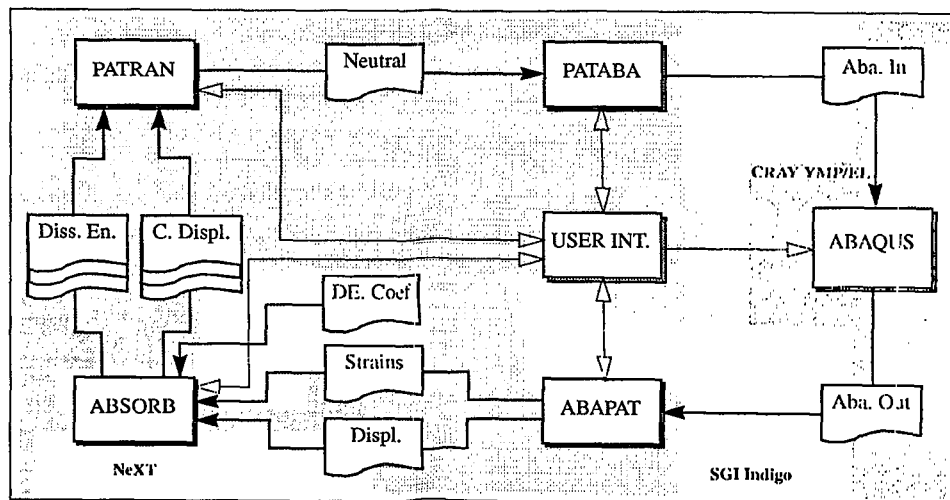


Fig. 1. Block diagram of the architecture of the structural simulator and computational resource allocation.

files to an "ABAQUS" input file. The output from "ABAQUS" is stored in a file that is subsequently converted to a strain file and a displacement file in "PATRAN" format by the "ABAPAT" process. The displacement files are identified by the suffix ".dis" and the strain files have the suffix ".els." At this stage, the strains and displacements can be visualized from "PATRAN" or be fed into the dissipated energy module "ABSORB" which runs on a "NeXT" computer and generates a spatial energy absorption map by associating a value of dissipated energy with each strain combination at every spatial evaluation point. The required dissipated energy values are computed by interpolation using the coefficients in the file "rmt.x.y.pred" that were produced by the process depicted in Fig. 16 of Part I [6]. Finally, the white arrows that connect the user interface module with the other simulator modules signify user control over these modules through both the user interface and the networking TCP/IP utilities that control data transfer between the involved computing platforms.

There is currently an extensive effort at NRL to develop various simulating environments that can operate on stand alone computational architectures. Simplified versions with multimedia characteristics already exist for "MS-Windows 3.1" machines, and more advanced versions exist for the "SGI" platform.

3. Composite specimens

The specimen used in the IPL tests is an example of a structural object. It has structural loads, i.e., the loads applied by the IPL actuators. It has a structural geometry, i.e., the geometry of the specimen, and it has a structural material, i.e., the material under investigation. At any point within the structural object, strains are induced that act upon the material. In this instance, strains induced by the actuator loads act upon the specimen material. The strains are occasionally the same at different points of the specimen, but in general they are not. The strains act upon the specimen material, changing it on occasion. When

the strains do change, the material shows the change by exhibiting a different elastic behavior suggesting reduction in local stiffness (softening). The experimentally determined dissipated energy is a measure of material softening. It is a nonlinear, monotonic function of the strains that act upon the material. As such, the material exhibits behavioral changes that may be unexpected. This application uses the IPL structural object to showcase the nature of the unexpected behavior.

Consider material 002 in Table 1 that was used as the straw person in this application. With a layup construction of $[(+30/-30)_4]_s$, this laminated composite material has piles constructed from AS1 carbon fibers, and 3501-6 epoxy resin. Load icons were employed in the figures of this application to facilitate recognition of the particular load combination being applied to a specimen. Five graphic symbols were used in combination to produce these icons. They are: a clockwise arrow to indicate clockwise motion of the movable boundary of the specimen; a counterclockwise arrow to indicate the opposite motion; an upwards-pointing arrow to indicate motion of the points of the movable boundary parallel to the y -axis; a downwards arrow for the opposite motion; and a right-pointing arrow to indicate motion of the points of the movable boundary parallel to the x -axis.

The interpretation of a particular combination of the graphic symbols is that the corresponding combination of IPL applied motion is applied proportionally to the specimen's movable boundary. The specimen, caught between its movable and immovable boundaries, deforms with a compatible motion. Loads that are proportional to each other are represented by the same icon. The particular magnitude of the proportional load is indicated individually, or by group where applicable. That specimen dissipated energy is a continuous nonlinear monotonic function of load displacement magnitude is an experimentally determined fact. The material dissipation energy is forced to be a continuous nonlinear monotonic function of strain magnitude. Though the specimen, undeniably, is nonlinear monotonic, the computed material dissipation function behaves that way by analytic design.

Fig. 2 depicts the loading case for load path 11 (1p-11). The load magnitudes shown are 20, 40, and 60 percent of the maximum boundary motion applied during the experiment for this particular

specimen. Fig. 2 also illustrates the monotonic nature of dissipated energy with respect to strains. Dissipated energy never decreases with increasing magnitudes of loading. It is also apparent

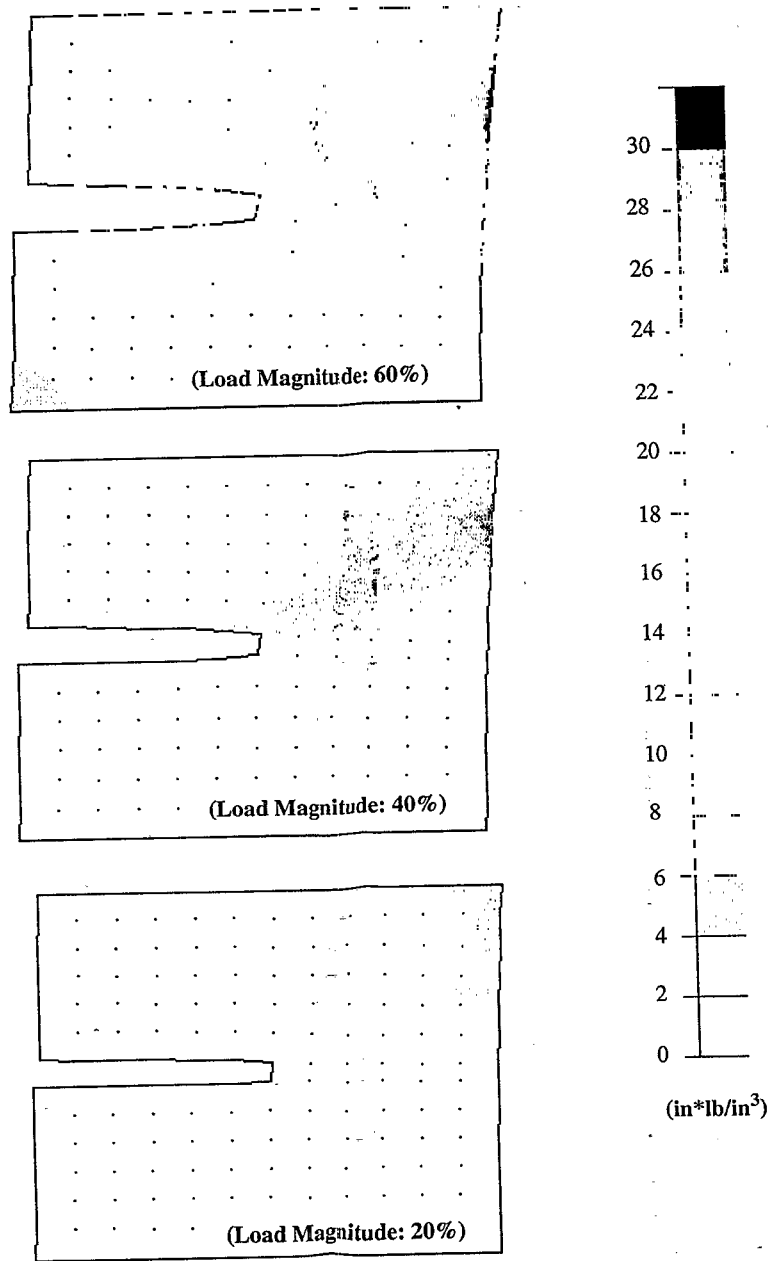


Fig. 2. Distributions of dissipated energy density on the deformed specimen for loading path 11, material 002 (AS1/3506-1 [+/- 30°]) for three different magnitudes of loading.

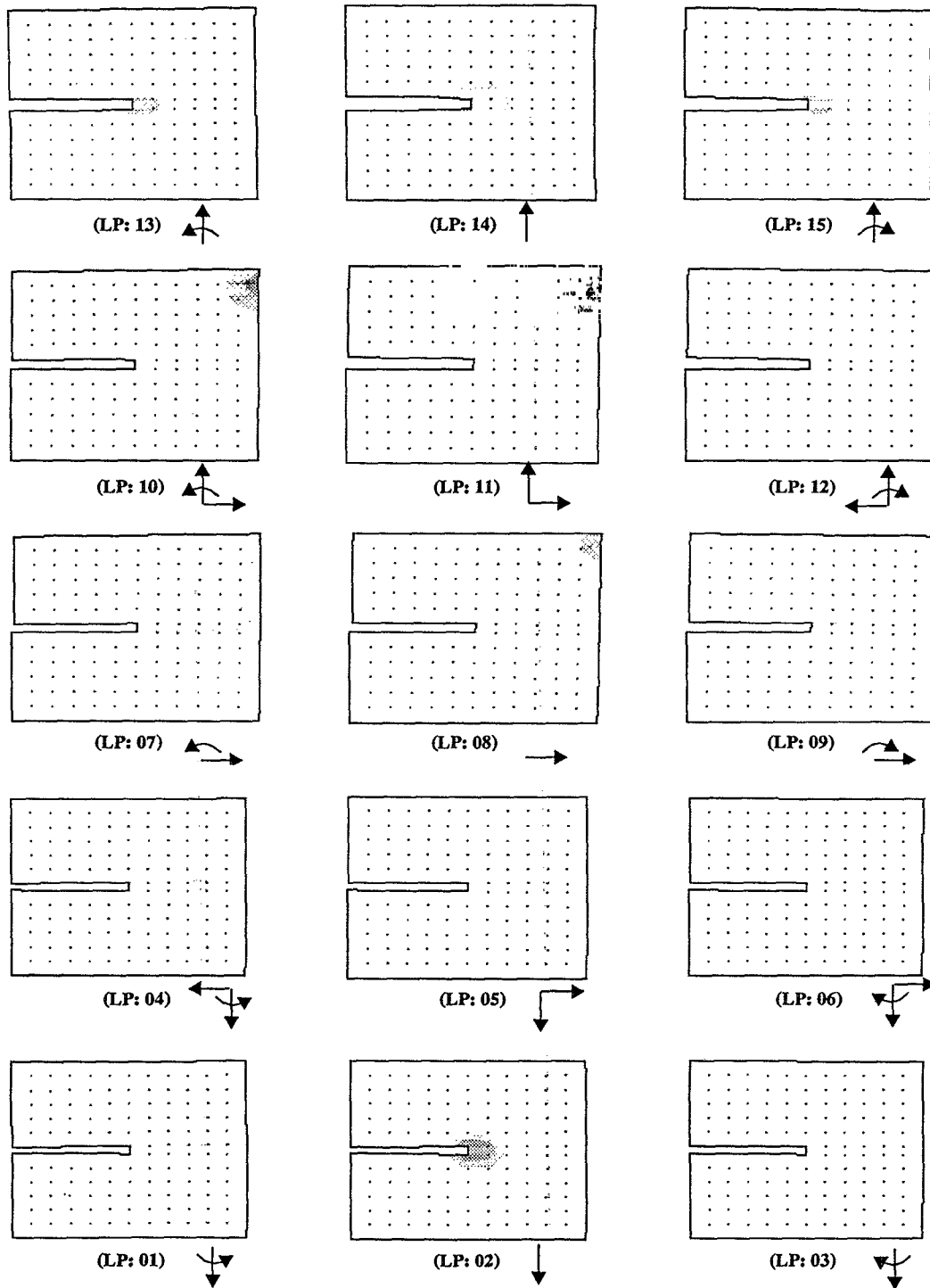


Fig. 3. Distributions of dissipated energy density on the deformed specimen for load magnitude 2, material 002 (AS1/3506-1 [$\pm 30^\circ$]), for each of the load paths 1–15.

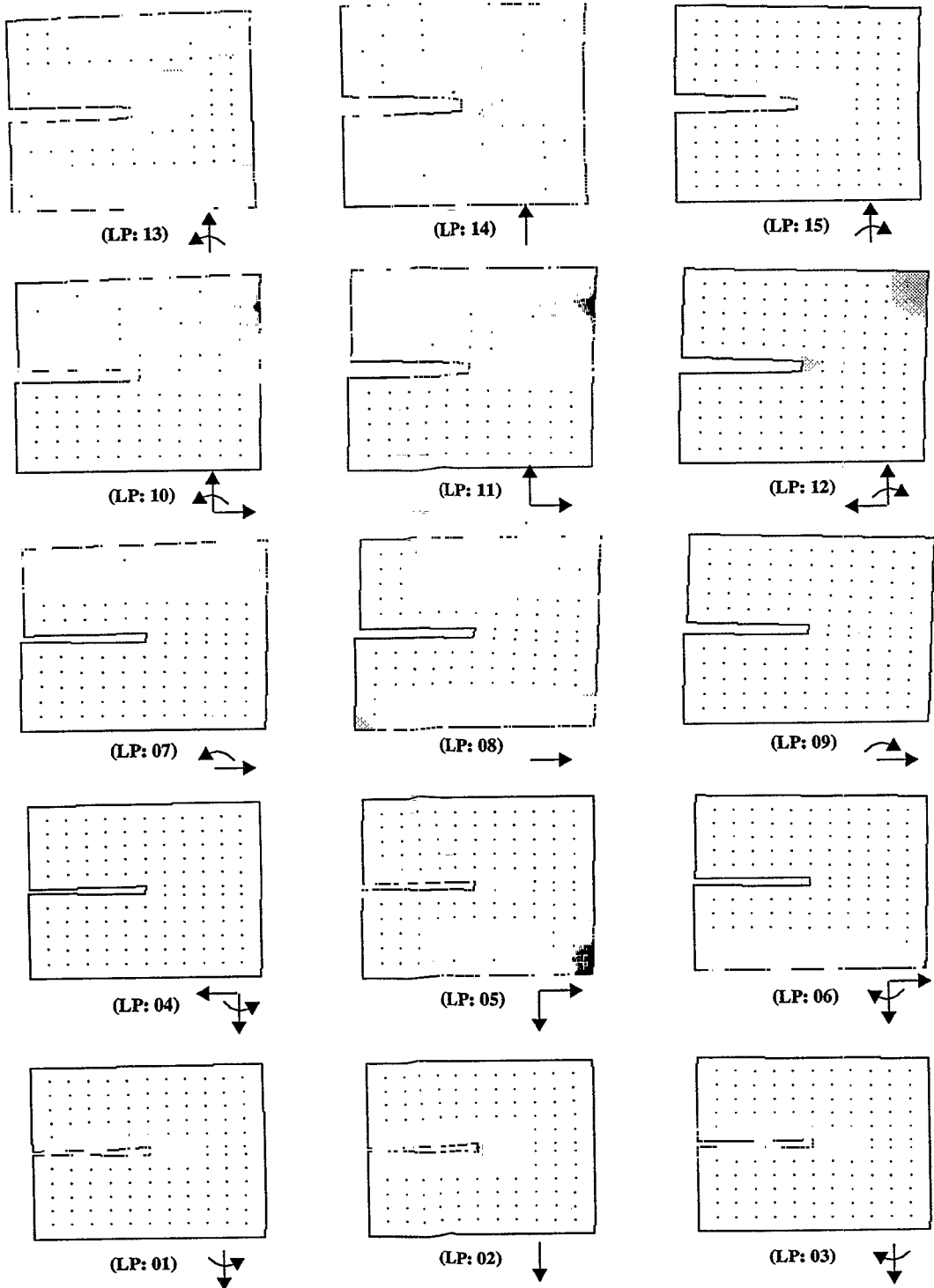


Fig. 4. Distributions of dissipated energy density on the deformed specimen for load magnitude 3, material 002 (AS1/3506-1 [$\pm 30^\circ$]), for each of the load paths 1-15.

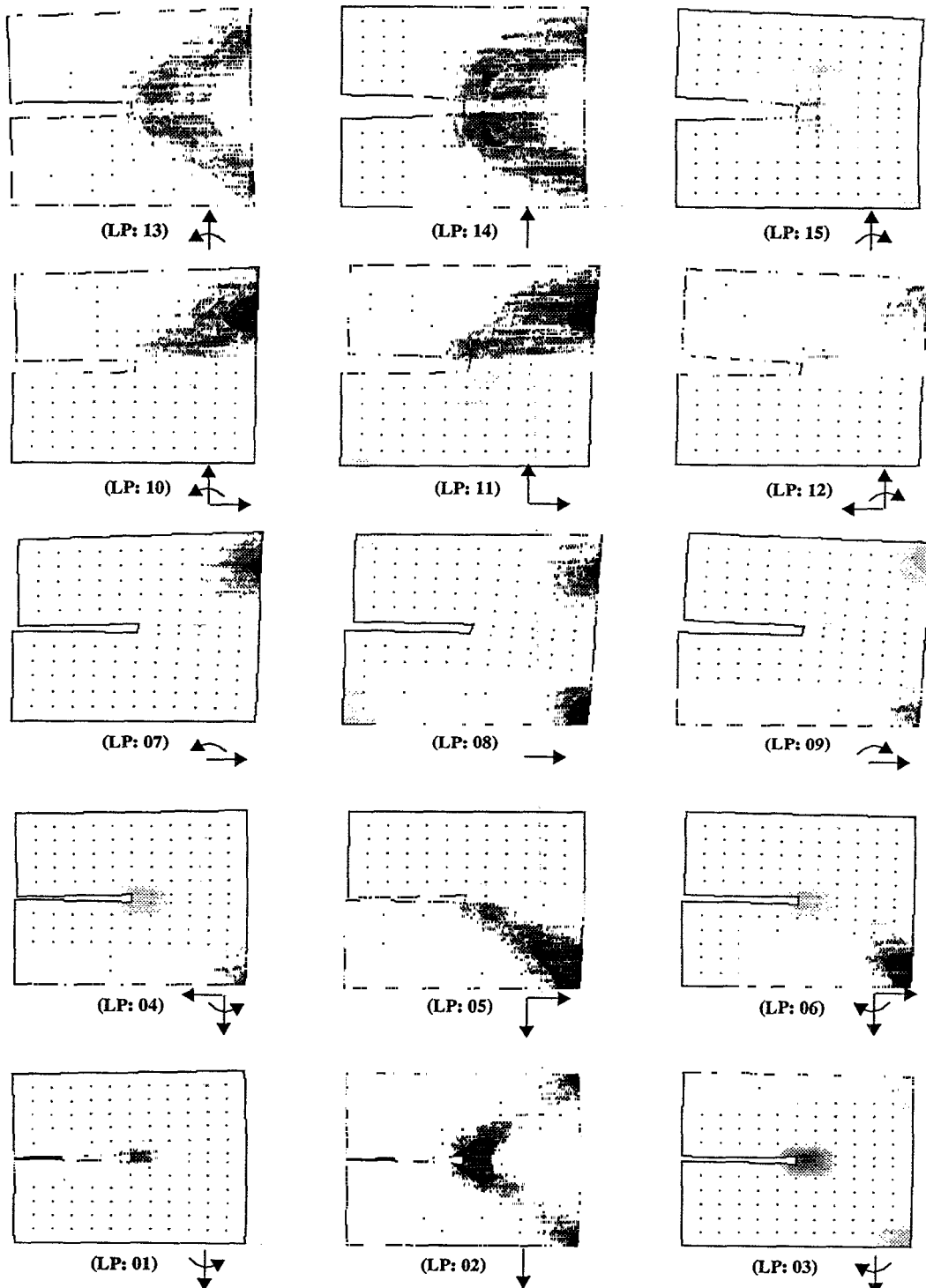


Fig. 5. Distributions of dissipated energy density on the deformed specimen for load magnitude 4, material 002 (AS1/3506-1 [$\pm 30^\circ$]), for each of the load paths 1-15.

here that the dissipated energy may not increase after reaching a certain magnitude of strain, and that a minimum magnitude of strain is required before the dissipated energy can become greater than zero. This observed behavior corresponds precisely to what is meant by the term a nonlinear monotonic function of strain magnitude.

To reiterate, that specimen dissipated energy is a continuous nonlinear function of load combination is an experimentally determined fact. In computing the material dissipation energy function from the specimen dissipated energy, the only analytic control exercised is to ensure continuous behavior with respect to the strain combination. Consequently, the nonlinear effect of strain combination as illustrated in Figs. 3, 4, and 5 is closely related to the experimentally observed behavior.

Figs. 3, 4, and 5 all depict the same set of the

15 different load combinations used in obtaining the experimental results. Fig. 3 is for the case of 20% of full load magnitude, while Fig. 4 is for 40%, and Fig. 5 for 60%. The effect of opening vs. closing motion (lp-14 vs. lp-2), which may be likened to tension vs. compression behavior, is quite distinctive. At the 20% level, both cases are indistinguishable. At the 40% load level, the opening or tension case has developed an extensive hot area from the notch tip out along the $\pm 30^\circ$ fiber directions all the way to the edge of the specimen, while the closing or compression case has changed only slightly. At the 60% load level, the situation has changed dramatically again. The compression case has developed a hot zone of the same configuration as that for tension. But while the zone for opening is diffuse, that for closing is concentrated at the notch and at the edge.

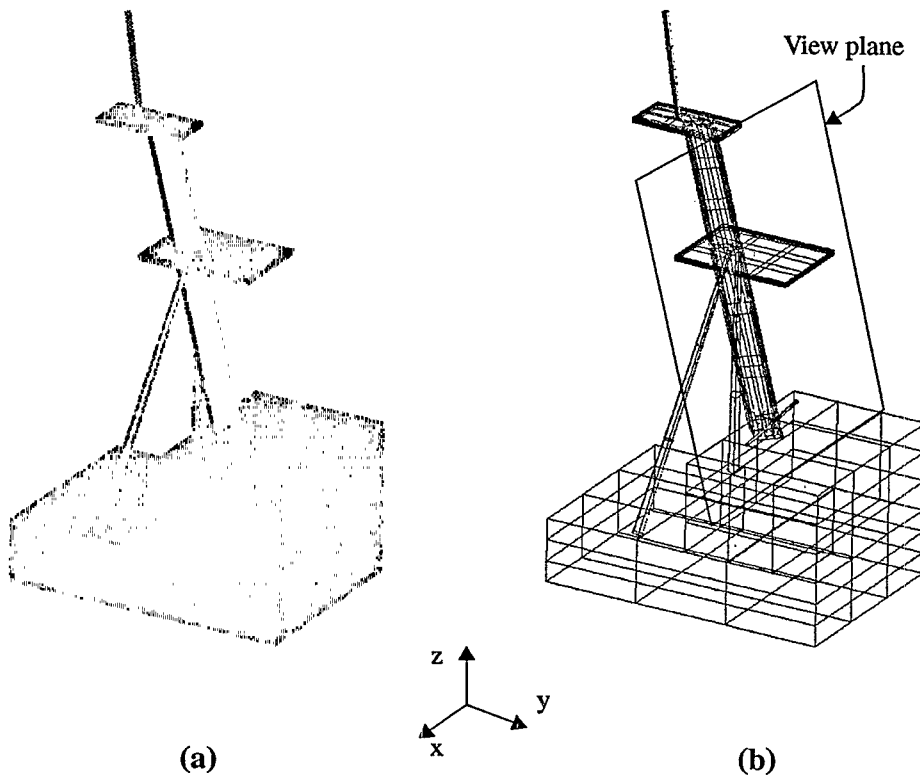


Fig. 6. Rendered view of (a) the mast structure and (b) wireframe view of the mast structure with the view plane used for displaying the dissipated energy density distributions.

The effect of opening, sliding, and closing load combinations (lp-14,lp-8,lp-2), demonstrates clearly the distinction between linear effect and nonlinear effect. The opening and sliding combinations is lp-11. Lp-14 and lp-8 both show extensive zones of nonzero dissipated energy in the lower half of the specimen. A linear effect would show dissipated energy as a proportional sum of the dissipated energy from cases lp-14 and lp-8. Clearly, lp-11 shows no nonzero dissipated energy in the lower half of the specimen. The effect is

typical of nonlinearity. The sliding, closing combination, lp-5, exhibits the same nonlinear effect.

The general assertion is that “if the IPL experiments were conducted using another specimen shape, then the material dissipation energy function would be the same”. In other words, the material behavior should be independent of the structure or of the loads that may be applied to that structure. If the preceding discussion and Part I [6] had been about this alternative experimental specimen, then the different specimen

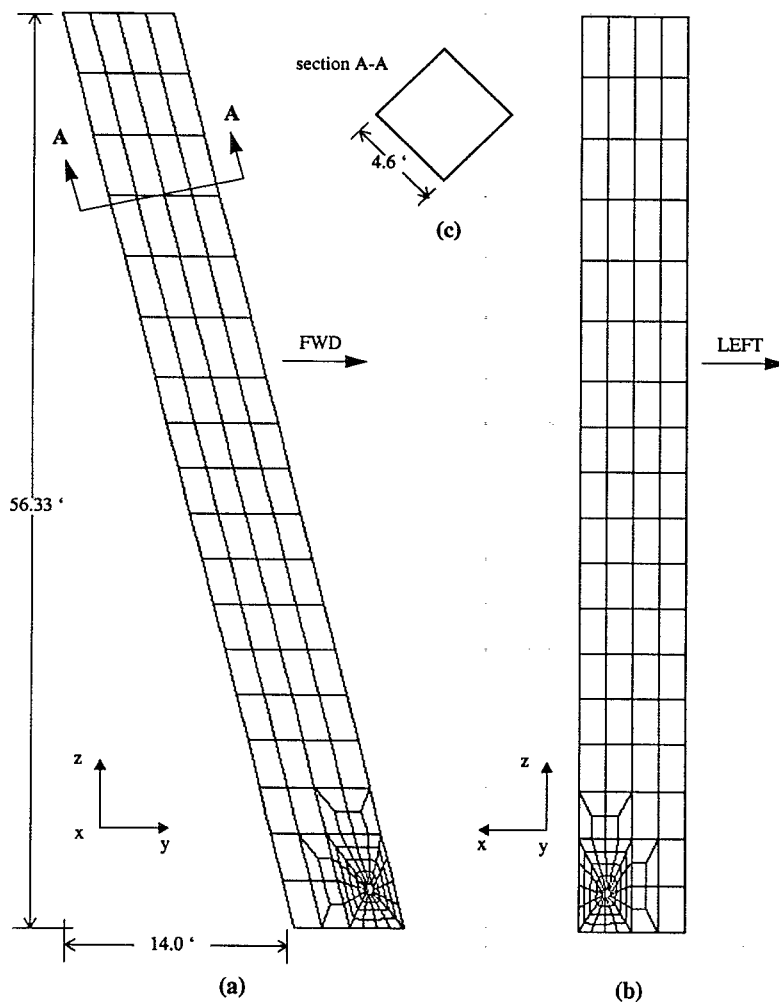


Fig. 7. Right side view of the finite element meshing and dimensions of the mast (a); front view of the mesh (b); cross section of the mast (c).

shape would have produced different strain distributions and consequently different material dissipated energy distributions. The same general continuous, nonlinear, monotonic nature of the material dissipation energy function would have been noted, but their distributions within the specimen would have been different. If a strong relationship had been drawn between the specimen, its loadings, and the consequent distributions of material dissipated energy from the cases presented, then a different strong relationship would have been drawn from consideration of the results for the alternative specimen.

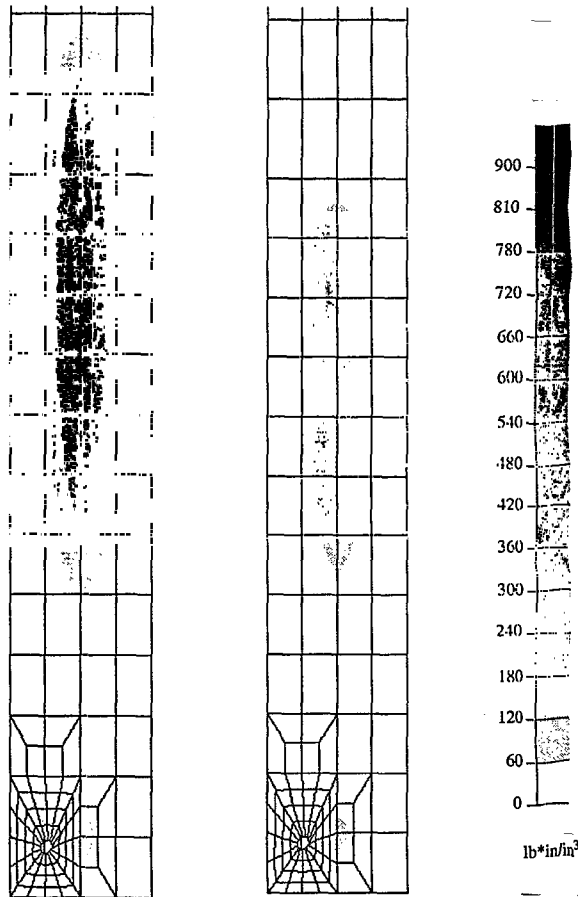


Fig. 8. Front views of dissipated energy density distributions of ship mast made out of thermoset material 007 (AS4/3501-6 [+/-60°]) (left) and out of thermoplastic material 040 (AS4/PEEK [+/-60°]) (right), for 1x the total loading corresponding of front wind.

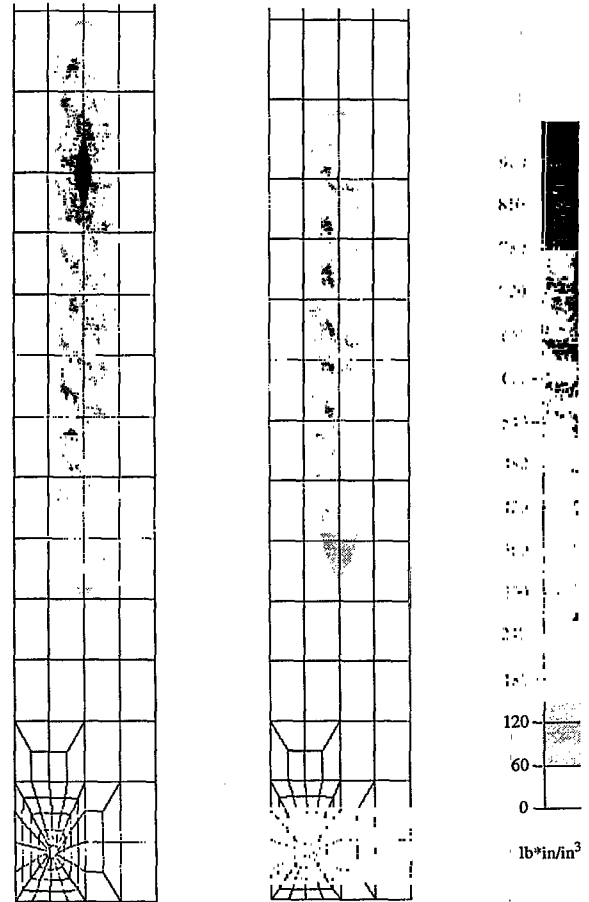


Fig. 9. Front views of dissipated energy density distributions of ship mast made out of thermoset material 007 (AS4/3501-6 [+/-60°]) (left) and out of thermoplastic material 040 (AS4/PEEK [+/-60°]) (right), for 2x the total loading corresponding of front wind.

The danger is in attempting to infer material behavior from specimen behavior, without regard to how the strains are distributed within that particular specimen.

4. Application to naval structures

Two specific naval structures have been chosen to demonstrate application of the dissipated energy density map distributions, to study effect of increasing loading and usage of different mate-

rials. These structures are a ship mast and an idealized submarine hull.

4.1. Ship mast

One of the design goals is to investigate the merits of using composite materials for ship masts. The primary reasons composite masts are being considered are weight reduction and favorable radar return characteristics. Traditional designs for metal masts were based on the assumption of linear elastic behavior and stress-based damage criteria; namely, that internal load-induced dam-

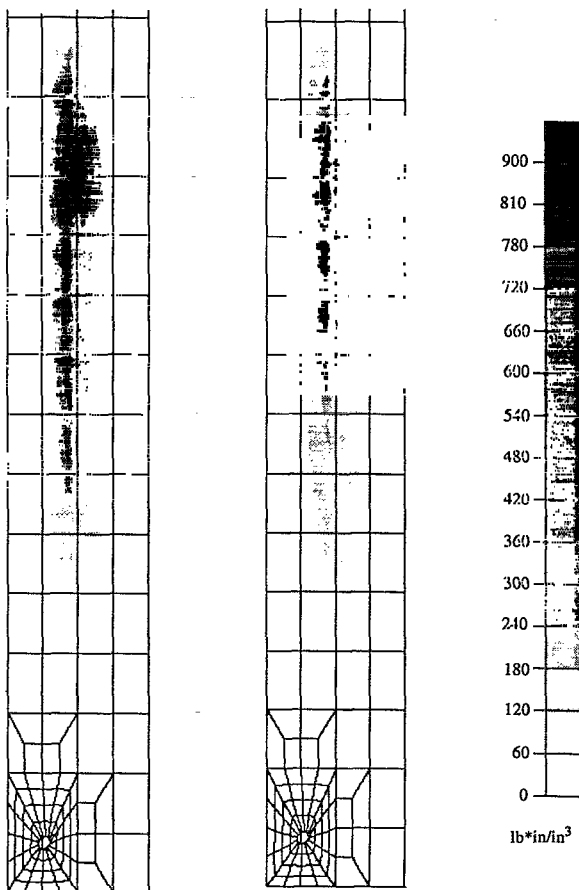


Fig. 10. Front views of dissipated energy density distributions of ship mast made out of thermoset material 007 (AS4/3501-6 [+/-60°]) (left) and out of thermoplastic material 040 (AS4/PEEK [+/-60°]) (right), for 3× the total loading corresponding to front wind.

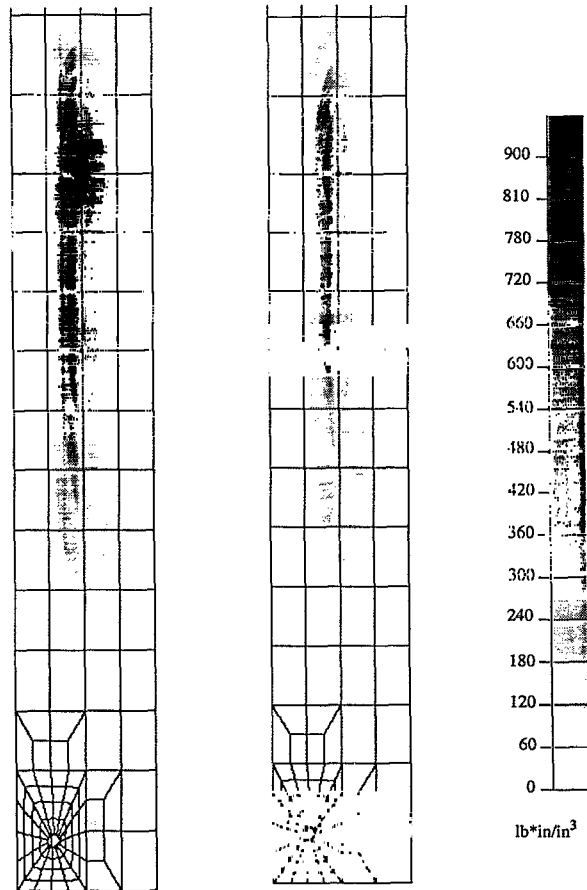


Fig. 11. Front views of dissipated energy density distributions of ship mast made out of thermoset material 007 (AS4/3501-6 [+/-60°]) (left) and out of thermoplastic material 040 (AS4/PEEK [+/-60°]) (right), for 4× the total loading corresponding to front wind.

age was assumed to occur whenever the stress exceeded a specified maximum stress set at 2.5 times the yield stress for the material used. As mentioned previously, such a simplistic view of failure behavior is not justified in composites, and a more realistic damage model such as the one being proposed in this study is required. The enhanced understanding provided by such a model should lead to lower safety factors and, therefore, more efficient mast designs. The structural response simulator together with a database of computed dissipated energy functions repre-

sent a unique medium to achieve the efficient design of composite masts.

The DDG-51 class of frigates was selected as a candidate ship for a representative mast installation. The geometry of the mast is that of a tripod mast with a rectangular box beam and two struts with two antenna platforms attached to it and the associated deckhouse as shown in Fig. 6. The design loads selected for this case were extracted from the "DDS-170" manual. For demonstration purposes, a wind load of 30 psf (lb/ft²) corresponding to a 90 kn head wind was selected. In addition, an inertial load of 0.6 g applied downwards to the center of gravity of the mast, or 0.2 g applied upwards on the center of gravity of the mast. A 500 lb antenna load was assumed to be applied at the upper platform and a 1000 lb antenna load applied at the lower platform of the mast were also considered. Only the case of head-on wind load is presented here, however.

The materials used for this simulation were item 007 (Resin 3501-6, Fiber AS4, Layup $\pm 60^\circ$) and item 040 (Resin PEEK, Fiber AS4, Layup $\pm 60^\circ$) as described in Table 1 of Part I [6]. These materials were selected to establish the relative merits of the thermoset 3501-6 resin material vs. the thermoplastic PEEK resin material. The material was composed of 130 successive

piles of 0.0075 in. each, thus accounting for a total thickness of 0.975 in. Fig. 7 shows the dimensions and the finite element mesh for the simulation of the mast structure itself. A total of 106 "ABAQUS" "QUAD" elements were used for the finite element idealization. In addition, battle damage was simulated by considering a 5 in. hole at the right side of the foot of the mast as shown in Fig. 7.

Figs. 8-11 present the simulation results for different loading and material choices as seen from the front of the mast in the region indicated in Fig. 6 with a rectangular window. All figures are fringe plots of the dissipated energy distribution over the structure. In all of these figures, the views on the left represent the dissipated energy distribution for the 3501-6 thermoset material, and the views on the right represent the dissipated energy distribution for the PEEK thermoplastic material.

The effect of applying an increasingly higher load corresponding to front wind is manifested as an increasingly higher distribution of fringes for higher levels of loading. Each one of these figures has been plotted for 1 \times , 2 \times , 3 \times , and 4 \times overload levels of the original 30 lb/ft² loading in the same order they appear in the document. Another characteristic of the response of the

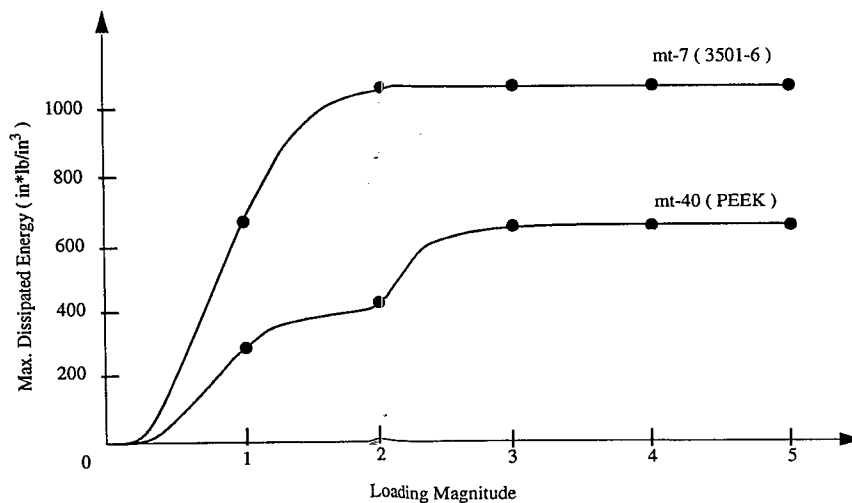


Fig. 12. Distribution of the maximum dissipated energy of the ship mast structure for materials 007 (AS4/3501-6 [$\pm 60^\circ$]) and 040 (AS4/PEEK [$\pm 60^\circ$]), vs. the loading magnitude.

structure due to the increasing load is the effect demonstrated in Fig. 12 where the maximum dissipated energy is plotted as a function of the load magnitude. That is, after a certain loading level, the material reaches a saturation level, where the dissipated energy in the material ceases to increase. This was the reason the distributions of overload magnitudes 4 and 5 were almost identical and, therefore, it seemed appropriate not to present the plotted distributions for loading magnitude 5. Evidence of this can be seen by comparing the dissipated energy distributions for loading magnitudes 3 and 4 in Figs. 8 and 11.

A significant observation is that the 3501-6 material seems to show a significantly higher propensity to go into its nonlinear region than does the PEEK material. This is evident from the higher number of fringes and their higher intensity as they appear on the 3501-6 distributions in Figs. 8–11 compared to those of the PEEK in Figs. 8–11. In addition, the 3501-6 material also has the tendency to dissipate higher amounts of dissipated energy as is shown by the saturation levels in Fig. 12. It is apparent from all these figures, that the mechanical damage, in terms of dissipated energy, caused by the round penetra-

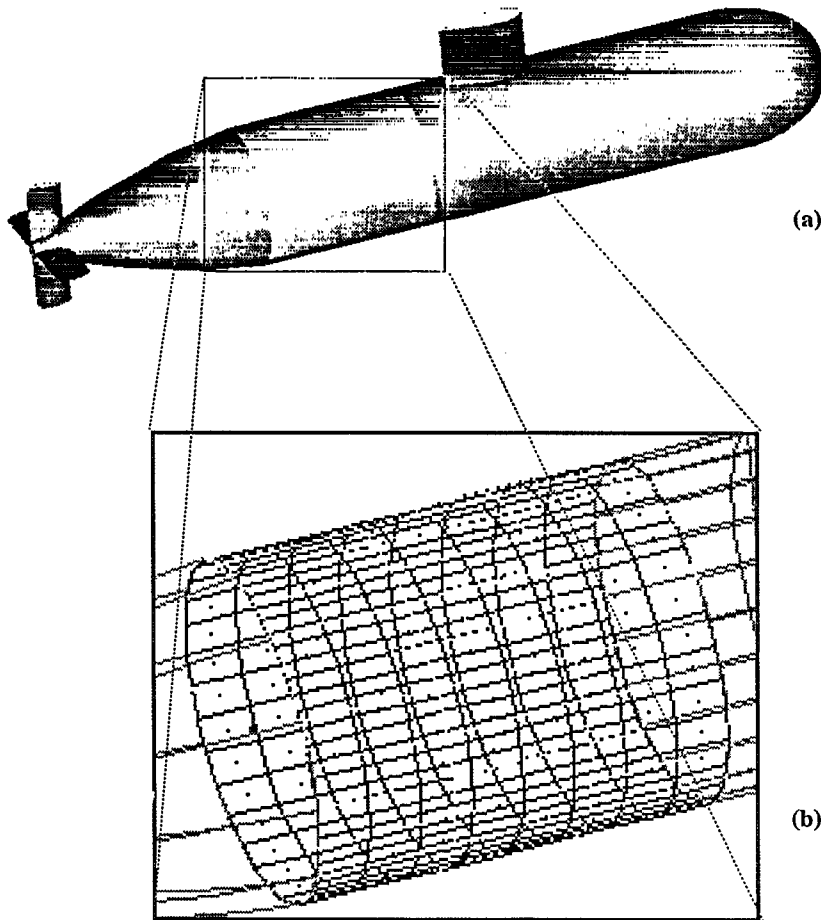


Fig. 13. Cylindrical shell as a section of (a) an idealized submarine, and (b) the corresponding finite element mesh.

tion on the left side of the base area of the mast is negligible compared to the one on the middle level of the structure.

4.2. Submarine Hull

An underwater structure, such as a submarine, is subject to a vast range of loads. These loads vary from underwater explosions, underwater wave actions, maneuvering loads, depth loads, to a whole variety of other types of loads. The survivability of the structure under these conditions is of prime importance. Since their invention, submarines have mainly been constructed from metals, but today, composites are being considered as a viable alternative. Dissipated en-

ergy offers a means of mapping out or hot spotting areas of concern on composite submarine structures. The structural loads, structural geometry, and the structural material act to produce strains throughout the structure that may induce changes in the material. Dissipated energy as a function of strain determines when a material will change from one elastic state to another, and is an important means of measuring both the extent of the material changes and the structural survivability.

Consider a generic submarine and, in particular, analyze the cylindrical hull section. The actual dimensions used are those of a generic dry dock shelter. The cylindrical shell idealization was selected as a simple showcase for dissipated

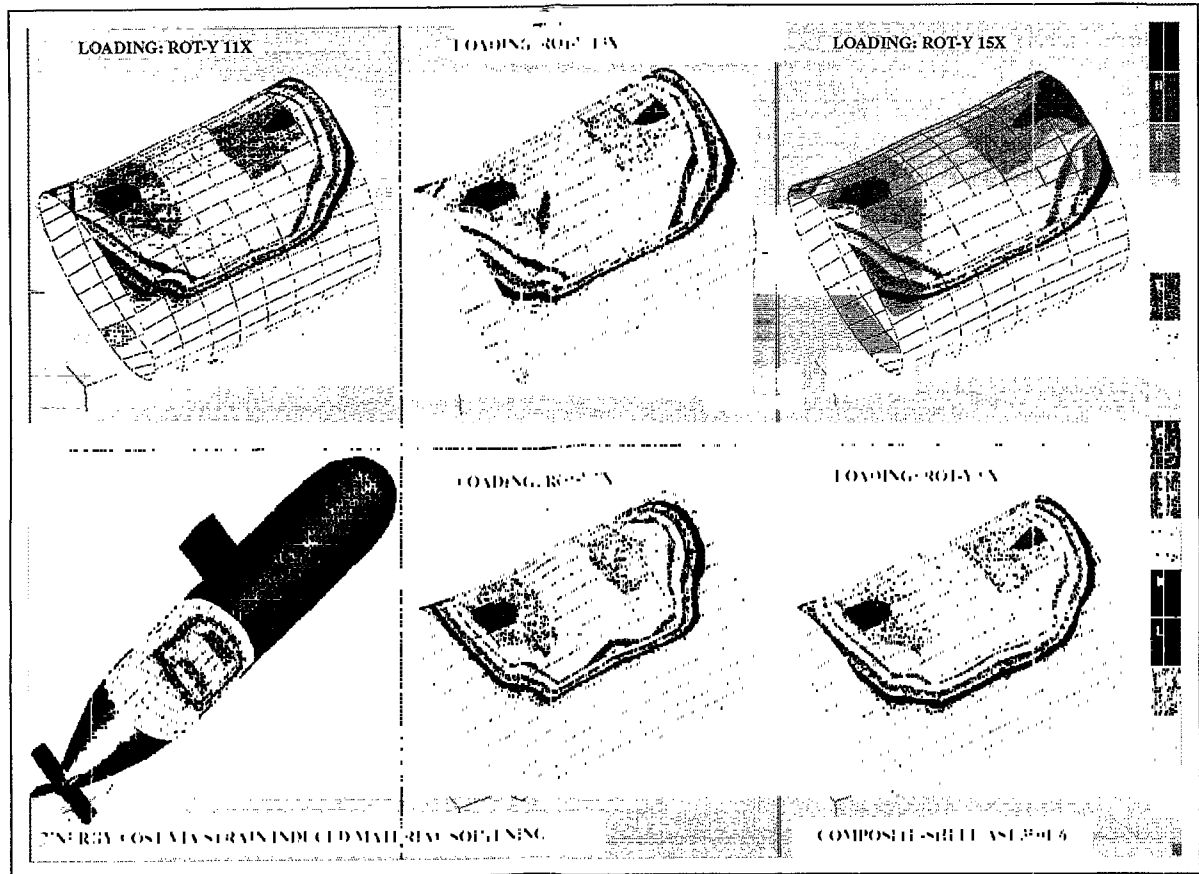


Fig. 14. Dissipated energy density distributions at the outer surface of the shell structure, for loading magnitudes of 7,9,11,13, and 15 times overload.

energy mapping. The finite element model used is shown in Fig. 13 and consists of 256 shell "QUAD" elements. The cylinder that was analyzed was 100 in. long, 80 in. diameter, and 1 in. thick. The boundary loading conditions were those induced by rigid body plane rotations of the ends of the cylinder. These loading conditions were chosen as a nominal representation of the kinds of loads that might be carried through to the cylinder by the rest of the submarine in response to bending loads about the vertical or y -axis. The shell material was a laminated graphite thermoset epoxy. The layers were oriented at $\pm 60^\circ$ to the longitudinal, or z -axis. The fibers were AS4 and the resin was a 3501-6 type epoxy. The finite

element code "ABAQUS" was used to determine the interior strain field. The strains as reported back by the code are for the Gauss integration points used by "ABAQUS" to determine the shell properties. Three integration points were used in this analysis, one point at the center of the laminate and two points at about an eighth of the thickness in from each side. In this case, the dissipated energy is not computed on a per ply basis, but rather on a smeared-out point basis, or a partial dissipated energy number at an integration point. Gaussian integration is then used to compute a total dissipated energy through the thickness. Both types of dissipated energy are illustrated in the following figures where the par-

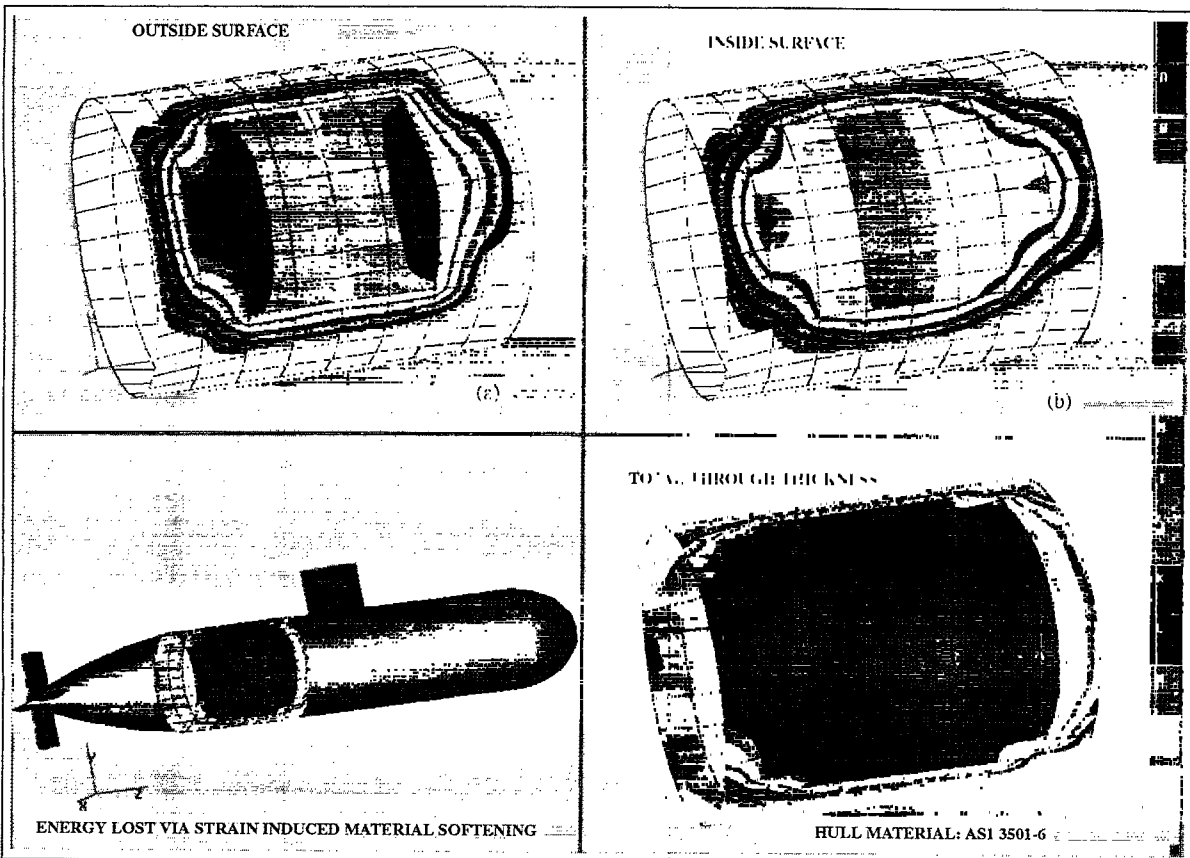


Fig. 15. Dissipated energy density distribution for (a) the inside surface of the shell, (b) the outside surface of the shell and (c) integrated through the thickness.

tial dissipated energy at the outer part of the shell is shown in Fig. 14 and total dissipated energy in Fig. 15.

Fig. 14 depicts the dissipated energy maps for overloads of 7X, 9X, 11X, 13X and 15X. The values shown are for partial dissipated energy close to the outer side of the shell. As can be seen in Fig. 14, the boundary of the hot-spotted zone (higher values of dissipated energy) at 7X overload is practically the same as at 15X overload. An observer may interpret this in several ways; however, it is reasonable to surmise that the damage as indicated by the hot-spotting is not going to grow unstably, and that regardless of the point of view taken as to the meaning of the damage, the material degrades only so far and thereafter gets no worse. Fig. 15 depicts the distribution of dissipated energy from below the inside surface, the outside surface, and throughout the thickness, i.e., partial vs. total viewpoints. The partial viewpoints show both similarities and differences. In both, the extent of the hot zone is roughly the same; however, each exhibits markedly different distributions within the zone.

The total dissipated energy viewpoint shows a larger hot zone than either of the partial dissipated energy maps. It also shows a rather constant value of dissipated energy over the area of the hot zone. From this an important inference may be drawn, that the nonlinear effect of strain on material loss of local stiffness, or change, may not be characterizable strictly on the basis of a partial or a total viewpoint.

5. Concluding remarks

The proposed procedure involves the determination of an energy density dissipation function which has the dimensions of energy per unit volume and is postulated to be a property of the material. Its volume integral equals the energy dissipated during loading because of the various internal failure events, and its value at any point in the material is regarded as a measure of load-induced internal damage. The energy dissipation function thus captures the collective behavior of these failure mechanisms without requiring an

explicit knowledge of these mechanisms, and, moreover, can also be related to local stiffness changes that lead to a form of nonlinear structural behavior. Determined are the energy dissipation function from data obtained by means of an extensive series of tests performed with NRL's In-Plane Loader, which is a computer-controlled testing machine capable of producing multiple combinations of opening/closing, sliding, and rotating boundary displacements.

Application of the method makes use of a computational approach packaged as a material response simulator that simulates the structural response of several structures of interest. These are the test specimen itself, a ship's mast, and a cylindrical shell representing an idealized section of a submarine hull. A number of different composite material systems are considered and spatial maps of the dissipation function (softening maps) are produced for various loading magnitudes. These softening maps illustrate how the energy consumed by the various internal failure events is dissipated within the structure.

Acknowledgements

The authors wish to acknowledge past and current financial support of the following Navy organizations and the indicated program managers:

Office of Naval Technology (J.J. Kelly³ and I.L. Caplan³ (DTRC Block Manager); Strategic Systems Project Office (E.L. Throckmorton³, R. Kinert, and F. Vondersmith); Naval Air Systems Command (C.F. Bersch); Naval Sea Systems Command (H.H. Vanderveldt, C. Zanis, W.R. Graner, and T.F. White).

The authors also wish to acknowledge helpful technical discussions with H. Marshall, Lockheed Palo Alto Research Laboratory, and J. Pitman, Gibbs and Cox Inc.

³ Current Program Managers.

References

- [1] R. Badaliance and H.D. Hill, Damage mechanisms and life prediction of graphite/epoxy composites, in: *STP775 Damage in Composite Materials*, ed. K.L. Reifsnider (ASTM, Philadelphia, PA, 1982) pp. 229–242.
- [2] J.E. Masters and K.L. Reifsnider, An investigation of cumulative damage development in quasi-iso-tropic graphite/epoxy, in: *STP775 Damage in Composite Materials*, ed. K.L. Reifsnider (ASTM, Philadelphia, PA, 1982) pp. 40–62.
- [3] A. Highsmith and K.L. Reifsnider, Stiffness-reduction mechanisms in composite laminates, in: *STP775 Damage in Composite Materials*, ed. K.L. Reifsnider (ASTM, Philadelphia, PA, 1982) pp. 103–117.
- [4] G.C. Sih, Impact damage of laminated composites with energy dissipation: Part I. Nonhomogeneous characteristics, *J. Theoret. and Appl. Fract. Mech.* 22, No. 3, to be published.
- [5] G.C. Sih, Impact damage of laminated composites with energy dissipation: Part II. damage evolution, *J. Theor. and Appl. Fract. Mech.* 22, No. 3, to be published.
- [6] P.W. Mast, G.E. Nash, J.G. Michopoulos, R. Thomas, R. Badaliance and I. Wolock, Characterization of strain-induced damage in composites based on the dissipated energy density: Part I. Basic scheme and information, this issue *J. Theor. and Appl. Fract. Mech.* 22, 71–96 (1995).
- [7] J.G. Michopoulos, G.C. Sih, S.C. Chou and J.F. Dignam, Energy dissipation in highly compressed cylindrical bar specimens, *J. Theoret. and Appl. Fract. Mech.* 2, 105–110 (1984).
- [8] G.C. Sih, Thermal/Mechanical Interaction Associated with the Micromechanisms of Material Behavior, Institute of Fracture and Solid Mechanics, Lehigh University, Bethlehem, PA (1987).
- [9] G.C. Sih, D.Y. Tzou and J.G. Michopoulos, Secondary temperature fluctuation in cracked 1020 steel specimen loaded monotonically, *J. Theoret. and Appl. Fracture Mech.* 7, 74–87 (1987).
- [10] E.T. Onat and F.A. Leckie, Representation of mechanical behavior in the presence of changing internal structure, *J. Appl. Mech.* 55, 1 (1988).